extensively investigated since the mid-1990s at the level of animal experiments. Cells harvested in primary cultures of heart muscle cells obtained from the fetus or the neonate were transplanted into the heart of sexually mature animals, and the transplantation was shown to improve post-infarction cardiac function. Clinical experience with the transplantation of fetal midbrain obtained through artificial termination of pregnancy into patients with Parkinson's disease has yielded some gratifying therapeutic results. The amount of cell transplants required is apparently greater in the case of cardiomyocyte transplantation, so that it is not practical to use aborted fetuses as the source.

Regenerated cardiomyocytes derived from ES cells, when transplanted, reportedly proved to electrically bound to recipient myocardium and contract synchronously with surrounding cells, thus fueling hopes for the use of regenerated cardiomyocytes. Our experience with regenerated cardiomyocyte transplantation into the hearts of adult patients showed long-term engraftment with gratifying outcomes. However, there have been reports demonstrating that the number of cardiomyocytes taken as compared to that of cardiomyocytes transplanted diminished due to cellular necrosis during the course of engraftment. Further study is needed, including assessments of transplantation methods.

Problems Associated with Myocardial Regeneration and Future Prospects

To bring regenerative cardiomyocyte transplantation to realization requires securing regenerated cardiomyocytes and supplying those cells safely and at moderate expense. When adult stem cells and ES cells are compared, this author's view is that the latter will come into use earlier in the future. Supply of regenerated cardiomyocytes derived from ES cells will become a reality within several years. Major problems are rejection reactions and method of transplantation. To avoid rejection, it is essential to transplant the nucleus of a somatic cell into an egg cell, as shown in Fig. 1. The nuclear transplantation eventually has a close bearing upon the matter of human cloning, therefore it is important to hold nationwide discussion of this ethical problem.

REFERENCES

1) Makino, S., Fukuda, K., Miyoshi, S. *et al.*: Cardiomyocytes can be generated from marrow stromal cells *in vitro*. *J Clin Invest* 1999; 103: 687–705.
2) Hakuno, D., Fukuda, K., Makino, S. *et al.*: Bone marrow-derived regenerated cardiomyocytes (CMG Cells) express functional adrenergic and muscarinic receptors. *Circulation* 2002; 106: 380–386.
3) Fukuda, K.: Differentiation from bone marrow mesenchymal stem cells into cardiomyocytes. *In:* Asajima, M., Iwata, H., Ueda, M. and Nakatsuji, N. (Eds.): "Regenerative medicine and life science — Reproductive engineering, stem cell engineering and tissue engineering", *Protein, Nucleic Acids and Enzymes*, (Special Issue), Kyoritsu Shuppan, Tokyo, 2000; 45 (13): 2078–2084. (in Japanese)

Nonhematopoietic mesenchymal stem cells can be mobilized and differentiate into cardiomyocytes after myocardial infarction

Hiroshi Kawada, Jun Fujita, Kentaro Kinjo, Yumi Matsuzaki, Mitsuyo Tsuma, Hiroko Miyatake, Yukari Muguruma, Kosuke Tsuboi, Yuji Itabashi, Yasuo Ikeda, Satoshi Ogawa, Hideyuki Okano, Tomomitsu Hotta, Kiyoshi Ando, and Keiichi Fukuda

Bone marrow (BM) cells are reported to contribute to the process of regeneration following myocardial infarction. However, the responsible BM cells have not been fully identified. Here, we used 2 independent clonal studies to determine the origin of bone marrow (BM)–derived cardiomyocytes. First, we transplanted single CD34$^-$ c-kit$^+$Sca-1$^+$ lineage$^-$ side population (CD34$^-$KSL-SP) cells or whole BM cells from mice ubiquitously expressing enhanced green fluorescent protein (EGFP) into lethally irradiated mice, induced myocardial infarction (MI), and treated the animals with granulocyte colony-stimulating factor (G-CSF) to mobilize stem cells to the damaged myocardium. At 8 weeks after MI, from 100 specimens we counted only 3 EGFP$^+$ actinin$^+$ cells in myocardium of CD34$^-$ KSL-SP cells in mice that received transplants, but more than 5000 EGFP$^+$ actinin$^+$ cells in whole BM cell in mice that received transplants, suggesting that most of EGFP$^+$ actinin$^+$ cells were derived from nonhematopoietic BM cells. Next, clonally purified nonhematopoietic mesenchymal stem cells (MSCs), cardiomyogenic (CMG) cells, that expressed EGFP in the cardiomyocyte-specific manner were transplanted directly into BM of lethally irradiated mice, MI was induced, and they were treated with G-CSF. EGFP$^+$ actinin$^+$ cells were observed in the ischemic myocardium, indicating that CMG cells had been mobilized and differentiated into cardiomyocytes. Together, these results suggest that the origin of the vast majority of BM-derived cardiomyocytes is MSCs. (Blood. 2004;104:3581-3587)

Introduction

Recent studies have suggested that bone marrow (BM) cells can contribute to regeneration processes in various tissues.[1,2] Cardiomyocytes derived from BM cells have been observed after myocardial infarction (MI),[3,4] and BM-derived cells mobilized by cytokines were capable of regenerating the myocardial tissue, leading to an improvement in survival and cardiac function after MI.[5] BM contains both hematopoietic and nonhematopoietic cells, and the origin of the BM cells with the ability to repair damaged myocardial tissue remains unknown. The identification of specific cell types involved in myocardial repair is a crucial step toward the development of effective stem cell–based therapies for MI.

The most likely candidates for the BM-derived stem cells with the ability to regenerate myocardial tissue are hematopoietic stem cells (HSCs)[3-5] and nonhematopoietic mesenchymal stem cells (MSCs).[6-10] Alvarez-Dolado et al recently demonstrated that BM-derived cardiomyocytes sporadically detected in noninfarcted mice were exclusively generated by fusion with donor CD45$^+$ cells, possibly hematopoietic cells,[11] suggesting that the so-called phenomenon of HSC "plasticity" might result from the fusion of HSCs with cells residing in the target tissue. Two recent studies reported that HSCs are unable to differentiate into cardiomyocytes in vivo even after MI.[12,13] MSCs also are candidates for the regeneration of cardiomyocytes in vivo; we previously reported that BM-derived MSCs could differentiate into spontaneously beating cardiomyocytes in vitro,[6-8] and other groups have repaired the myocardium using MSC transplantation in vivo.[9,10]

The aim of this study is to determine the precise origin of the BM cells mobilized by cytokines to repair infarcted myocardium. We transplanted genetically marked single HSCs or clonal MSCs into lethally irradiated recipient mice, induced MI, treated the mice with granulocyte colony-stimulating factor (G-CSF), and analyzed the cardiac tissues. Our results suggest that MSCs are the predominant source of regenerated cardiomyocytes.

Materials and methods

Mice

C57BL/6 (B6) mice and C3H/He (C3H) mice were purchased at 6 to 8 weeks of age from Japan CLEA (Tokyo, Japan). B6 transgenic mice that ubiquitously expressed enhanced green fluorescent protein (EGFP) under

From the Division of Hematology, the Department of Medicine, Tokai University School of Medicine; Research Center for Regenerative Medicine, Tokai University School of Medicine; the Department of Internal Medicine, Keio University School of Medicine; the Institute for Advanced Cardiac Therapeutics, Keio University School of Medicine; Core Research for Evolutional Science and Technology-Japan Science and Technology and Department of Physiology, Keio University School of Medicine, Japan.

Submitted April 19, 2004; accepted July 24, 2004. Prepublished online as *Blood* First Edition Paper, August 5, 2004; DOI 10.1182/blood-2004-04-1488.

Supported by grants from the Ministry of Education, Science and Culture; and the Ministry of Welfare and Labor, Japan; as well as grants from the 21st Century Center of Excellence Program of the Ministry of Education, Science and Culture of Japan to Keio University and Tokai University.

H. K., J. F., and K. K. contributed equally to this paper.

An Inside *Blood* analysis of this article appears in the front of this issue.

Reprints: Keiichi Fukuda, Department of Internal Medicine, Keio University School of Medicine, 35 Shinanomachi, Shinjuku-ku, Tokyo 160-8582, Japan; e-mail: kfukuda@sc.itc.keio.ac.jp or Kiyoshi Ando, Department of Medicine, Tokai University of Medicine, Bohseidai, Isehara, Kanagawa 259-1193, Japan; e-mail: andok@keyaki.cc.u-tokai.ac.jp.

The publication costs of this article were defrayed in part by page charge payment. Therefore, and solely to indicate this fact, this article is hereby marked "advertisement" in accordance with 18 U.S.C. section 1734.

the control of the CAG promoter[14] were used as the BM donor in the transplantation studies using B6 mice. All the transgenic EGFP mice used in this study were heterozygous for the transgene.

Isolation of CD34⁻c-kit⁺Sca-1⁺ lineage⁻ SP cells (CD34⁻KSL-SP cells)

The isolation of the CD34⁻c-kit⁺Sca-1⁺ lineage⁻ SP cells was previously described.[15] Briefly, BM cells suspended at 1×10^6 cells/mL in HBSS+ (calcium- and magnesium-free Hanks balanced salt solution supplemented with 2% fetal calf serum [FCS], 10 mM HEPES [*N*-2-hydroxyethylpiperazine-*N*'-2-ethanesulfonic acid], 100 U/mL penicillin, and 100 μg/mL streptomycin) were incubated with 5 mg/mL Hoechst 33342 (Sigma Aldrich, St Louis, MO) for 60 minutes at 37°C. After washing, the cells were resuspended in ice cold HBSS+ at a cell density of 10^7 cells/mL and then stained for 30 minutes on ice with various monoclonal antibodies, including biotinylated CD34, allophycocyanin (APC)–conjugated c-kit, phycoerythrin (PE)–conjugated Sca-1, and PE-Cy5–conjugated lineage markers (Gr-1, Mac-1, B220, CD3, TER119). The biotinylated antibodies were visualized using PharRed (APC-Cy7)–conjugated streptavidin. All of these reagents were purchased from BD PharMingen (San Diego, CA). Cell sorting was performed using a triple laser MoFlo (Cytomation, CO) using Summit software. Hoechst 33342 was excited at 350 nm, and the fluorescence emission was detected using 405/BP30 and 570/BP20 optical filters against Hoechst blue and Hoechst red, respectively, and a 555-nm long-pass dichroic mirror (Omega Optical, Brattleboro, VT) to separate the emission wavelengths. Both Hoechst blue and red fluorescence were shown on a linear scale. After collecting 10^5 events, the side population (SP) was defined as described previously, and additional gates were defined as positive for Sca-1 and c-kit and negative for CD34 and lineage markers according to the isotype control fluorescence intensity. Populations of CD34⁻KSL-SP cells with 99% purity were routinely prepared using this method. Single CD34⁻KSL-SP cells derived from transgenic EGFP mice were sorted directly into separate wells of a 96-well plate containing 100 μL HBSS+ using a CyClone automated cell deposition unit.

HSC transplantation

Single CD34⁻KSL-SP cells or 5×10^6 whole BM cells from transgenic EGFP mice were injected intravenously into the retro-orbital plexus of etherized recipient B6 mice that had been lethally irradiated with a dose of 10.5 Gy (Figure 1A). For radioprotection, the single CD34⁻KSL-SP cells were transplanted along with 2×10^5 whole BM cells as radioprotective cells from B6 mice that did not carry the CAG-EGFP transgene. Three months after BM transplantation, peripheral blood samples were collected from the recipient mice, and the erythrocytes in the samples were depleted using Ficoll-Paque. Dual-laser fluorescence-activated cell-sorter scanner (FACS) analysis was performed using a FACS Calibur (Becton Dickinson, San Jose, CA). Donor BM–derived cells were determined by the fluorescent intensity of the EGFP, compared with wild-type cells, and mice engrafted with more than 50% of the EGFP⁻ cells were used for the experiments.

Myocardial infarction and mobilization of BM cells

The recipient mice were intubated and anesthetized with 0.5% isofluorane gas. After left thoracotomy, the left ventricle was exposed and the left coronary artery was ligated. Twenty-four hours later, the mice were subcutaneously injected with 300 μg/kg of recombinant human G-CSF dissolved in saline solution once a day for 10 consecutive days. Control mice received a saline solution without G-CSF.

Immunohistological studies

Hearts were perfused from the apex with phosphate-buffered saline (PBS) and perfusion fixed with 4% paraformaldehyde/PBS. They were then dissected, immersion fixed overnight at 4°C in 4% paraformaldehyde, embedded in Optimal Cutting Temperature (OCT) Compound (TED PELLA, Redding, CA), and quickly frozen in liquid nitrogen. Cryostat sections (6 μm thick) were stained overnight at 4°C using specific antibodies. Anti-GFP (MBL, Nagoya, Japan), anti–α-actinin (Sigma Aldrich), anti–sarcomeric myosin (MF20), anti–cardiac troponin I (Santa Cruz Biotechnology, Santa Cruz, CA), anti-GATA4 (Santa Cruz), and anti-CD45 (BD Pharmingen, San Diego, CA) were used to identify EGFP⁺ cells, cardiomyocytes, and hematopoietic cells. The sections were incubated with secondary antibodies conjugated with Alexa 488 or 594 (Molecular Probes, Eugene, OR). Nuclei were stained with TOTO-3 (Molecular Probes). Slides were observed under a confocal laser scanning microscope (LSM 510 META; Carl Zeiss, Jena, Germany). In some experiments, the liver, kidney, brain, skeletal muscle, and spleen of recipient mice also were analyzed by immunofluorescence photography. To observe the bone marrow cavity, bone tissue was fixed with 10% formaldehyde and decalcified in K-CX solution (Falma, Tokyo, Japan) at

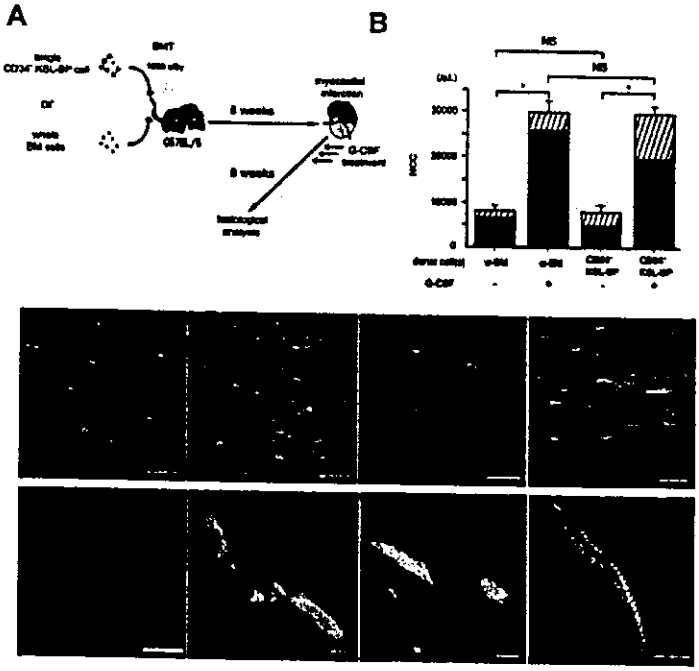

Figure 1. G-CSF–induced mobilization of BM cells in mice receiving transplants of single CD34⁻c-kit⁺Sca-1⁺ lineage⁻ side population (CD34⁻KSL-SP) cells or whole BM cells following MI. (A) Experimental protocol. Single EGFP⁻ CD34⁻KSL-SP cells and radioprotective EGFP⁻ BM cells were transplanted into the recipient mice. (B) The nucleated cell counts (NCCs) for peripheral blood samples obtained 24 hours after the last injection of G-CSF (n = 10) or saline (n = 10) are shown. ■ indicates EGFP⁺ cells; ▨, EGFP⁻ cells. NS indicates not significant; $^*P < .0001$. Bars indicate the standard error. (C-F) Panels show representative results for immunofluorescent analysis using anti–GFP antibody and TOTO-3 dye in the hearts of mice receiving transplants of w-BM cells or single CD34⁻c-kit⁺Sca-1⁻ lineage⁻ side population (CD34⁻KSL-SP) cells separated from the BM of transgenic EGFP mice. The green and blue signals indicate EGFP and nuclei, respectively. Saline-treated mice (G-CSF[−] mice) (C) and G-CSF–treated mice (G-CSF (+) mice) (D) in the w-BM group. G-CSF(−) mice (E) and G-CSF (+) mice (F) in the CD34⁻KSL-SP group. Bars indicate 200 μm. (G) The control experiment using C57BL/6J mice as donors revealed that no green fluorescence was detected in the whole heart. Bar indicates 50 μm. (H-J) Coimmunostaining with anti-GFP and anti–actinin antibodies in the infarcted myocardium of G-CSF(+) mice transplanted with w-BM (H, I) or single CD34⁻KSL-SP cells (J). The green, red, and blue signals indicate EGFP, actinin, and nuclei, respectively. (H, I) In the w-BM group, some of the EGFP⁻ cells in the infarcted area were positive also for actinin and showed striation, indicating that they had differentiated into cardiomyocytes. (J) In contrast, very few EGFP⁺ actinin⁺ cells were seen in the infarcted area in the CD34⁻KSL-SP group. Bars indicate 50 μm (H, I) and 20 μm (J).

4°C for 2 days. Sections (3 μm) were incubated with anti–GFP antibody overnight at 4°C. A specific signal was visualized as a brown reaction product of peroxidase substrate 3,3′-diaminobenzidine (Sigma). Samples were counterstained with hematoxylin and eosin.

Adherent cell culture and immunocytochemistry

Twelve weeks after the transplantation of the single $CD34^-KSL$-SP cells or w-BM cells from transgenic mice that ubiquitously express EGFP,[14] peripheral blood samples were collected from the retro-orbital plexus of the recipients. If more than 80% of the donor-derived $EGFP^+$ cells were found in the peripheral blood, the mice were killed and the BM cells were flushed from the femurs and tibiae to prepare single-cell suspensions. After most of the erythrocytes were removed with Ficoll-Paque, 3×10^5 BM mononuclear cells were plated on the fibronectin-coated wells of 96-well plates (Costar, Cambridge, United Kingdom) and incubated in Dulbecco modified Eagle medium (DMEM) supplemented with 10% fetal bovine serum (FBS), 100 U/mL penicillin, and 100 μg/mL streptomycin at 37°C in a fully humidified atmosphere of 5% CO_2. The medium was exchanged every 2 to 3 days, and nonadherent cells were removed. The cultures were terminated 2 weeks after seeding by removal of the culture medium. The samples were flushed 3 times with PBS and fixed with 4% paraformaldehyde, then stained with rabbit anti–GFP antibody (1:1000 dilution, Molecular Probes) and visualized using a secondary antibody of Alexa Fluor 488–conjugated goat anti–rabbit IgG (1:1000 dilution, Molecular Probes). The specimens were also stained with PE-conjugated rat anti–mouse CD45 (1:1000 dilution; eBioscience, San Diego, CA) and Hoechst 33342 (Sigma Aldrich). The adherent cells in each plate were counted under a fluorescent microscope.

Differentiation cultures for osteoblasts and adipocytes

To induce osteocyte differentiation, the adherent cells were cultured on slides in DMEM with 10 mM β-glycerophosphate, 10^{-7} M dexamethasone, and 0.2 mM ascorbic acid (all from Sigma Aldrich); the media was changed every 3 to 4 days. After 14 days, osteoblast differentiation was confirmed using alkaline phosphatase enzymatic staining. For the alkaline phosphatase staining, cells were fixed with methanol at −20°C for 2 minutes and then washed in 100 mM Tris [tris(hydroxymethyl)aminomethane]-HCl (pH 9.5), 100 mM NaCl, and 10 mM $MgCl_2$ buffer (all from Sigma Aldrich) for 10 minutes. The slides were then stained with fast 5-bromo-4-chloro-3-indolyl phosphate and nitroblue tetrazolium alkaline phosphatase substrate (both from Sigma Aldrich) for 10 minutes and rinsed in distilled water. To induce adipocyte differentiation, the adherent cells were cultured with 10% horse serum or 100 ng/mL insulin and were maintained for 14 days on the slides, with medium exchanges every 3 to 4 days. After 14 days, we confirmed the differentiation of the cells to lipid-laden adipocytes by staining with oil-red. For the oil-red staining, the cells were fixed with methanol at −20°C for 2 minutes and then rinsed in 50% alcohol. Slides were stained in oil-red-O (Sigma Aldrich) for 10 minutes and rinsed in 50% alcohol. After rinsing in distilled water, slides were counterstained with Mayer hematoxylin (Sigma Aldrich) for 1 minute.

Transduction of CMG cells

CMG cells derived from C3H mice were cultured in Iscoves modified Dulbecco medium supplemented with 20% FBS, 100 U/mL penicillin, 100 μg/mL streptomycin, and 85 μg/mL amphotericin B on fibronectin-coated dishes at 33°C in 5% CO_2, as previously described.[6] In the experiments shown in Figure 2A, the CMG cells were transduced with the recombinant ecotropic retrovirus murine stem cell virus (MSCV)-EGFP[16] at multiplicity of infection (MOI) 10, and the $EGFP^+$ cells were sorted using a FACS Vantage (Becton Dickinson, Cockeysville, MD), as previously described.[17] In the experiments shown in Figure 3A, an expression vector, pMLC2v-EGFP, was constructed by cloning a 2.7-kb *Hin*dIII-*Eco*RI fragment of the rat MLC-2v promoter region[18,19] into the *Hin*dIII-*Eco*RI site of pEGFP-1 (Clontech, Palo Alto, CA) so that EGFP would be expressed under the control of the MLC-2v promoter. The MLC2v-EGFP plasmid was then transfected into the CMG cells by liposomal transfection. After culturing with 1000 μg/mL of G418 for 4 weeks, permanently transfected single

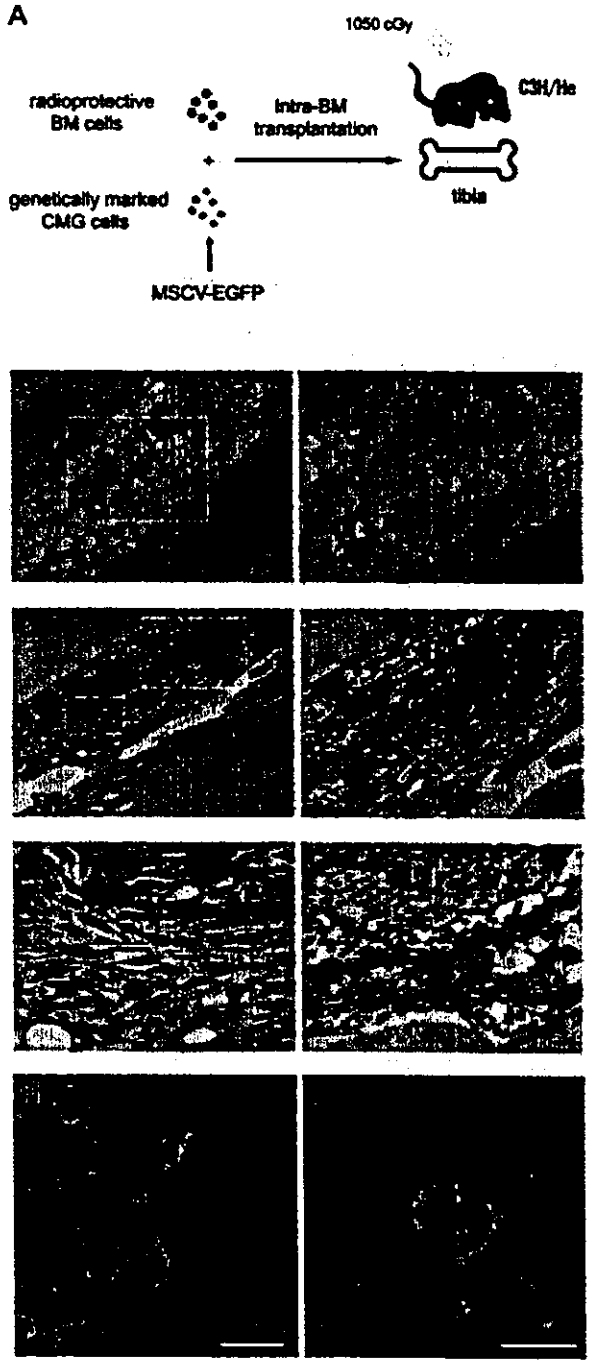

Figure 2. Engraftment and multilineage differentiation of clonal mesenchymal stem cells (CMG cells). (A) The experimental protocol for the intra-BM transplantation of CMG cells transfected with MSCV-EGFP is shown. (B-G) Transplanted CMG cells were observed in the recipients' BM. CMG cells were recognized as brown cells by immunohistochemistry. (B) CMG cells differentiated into adipocytes (arrows) (magnification, × 100). The rectangle in panel B is shown at a higher magnification (× 200) in panel C. (D) CMG cells also differentiated into osteocytes (arrows). Undifferentiated CMG cells exhibiting spindlelike shapes were also observed (arrowheads) (magnification, × 100). The rectangles in panel D are shown at higher magnifications in panels E (× 200) and F (× 400). (G) Undifferentiated CMG cells in other part (× 200). (H, I) CMG cells also were found in the liver (H) and kidney (I) by immunofluorescence photography. Bars indicate 10 μm. The green and blue signals indicate EGFP and nuclei, respectively.

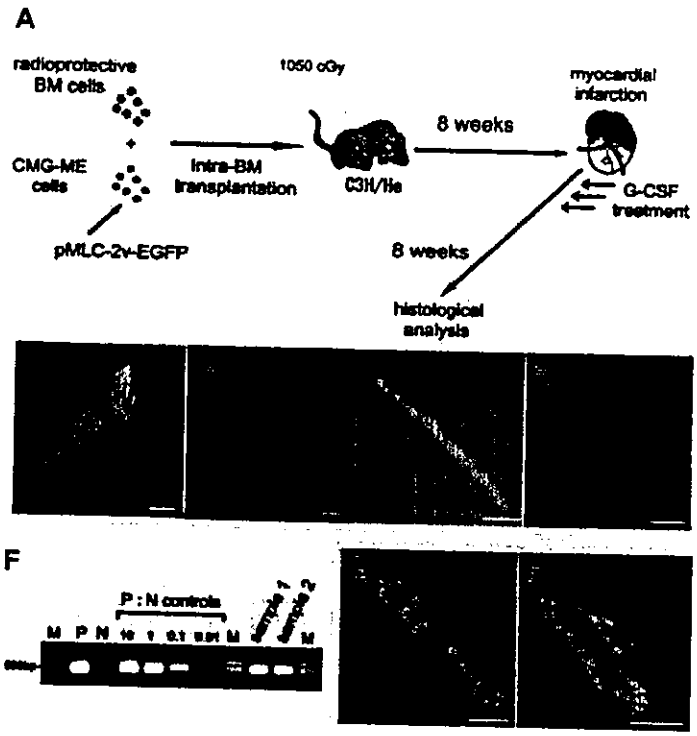

Figure 3. Mobilization and differentiation of mesenchymal stem cells (CMG cells) into cardiomyocytes in vitro and in vivo. (A) The experimental protocol is shown. The CMG-ME cells are CMG cells that have been permanently transfected with a plasmid-encoding EGFP driven by the myosin light chain promoter (pMLC2v-EGFP). (B,C) Cultured CMG-ME cells were treated with 5-azacytidine and immunoassayed with anti-GATA4 (red) antibody on the seventh day of culture. GATA4 was expressed in the CMG-ME cells. Some of the CMG-ME cells became EGFP$^+$ (green). (D,E) At 3 weeks, CMG-ME cells that were positive for both EGFP and actinin were observed, indicating that the cells had differentiated into cardiomyocytes. (F) The engraftment of CMG-ME cells into the recipients' BM was confirmed by PCR. Representative results using BM samples collected from recipient mice (samples 1 and 2) are shown. The transgene was clearly detected in the 2 samples. P indicates positive control (CMG-ME cells); N, negative control (CMG cells); M, marker. P:N controls are shown as the percentage with respect to the positive control. (G,H) The myocardium of infarcted mice that received transplants of CMG-ME cells was analyzed using immunofluorescent microscopy. The green, red, and blue signals indicate EGFP, actinin, and nuclei, respectively. EGFP$^+$ actinin$^+$ CMG-ME cells were observed in the myocardium, indicating that the CMG-ME cells had been mobilized into the ischemic myocardium. Actinin and EGFP expression, driven by the MLC-2v promoter, was detected, indicating that the cells had differentiated into cardiomyocytes. Bars indicate 10 μm.

cell–derived colonies were cloned and pooled (CMG-ME cells). For in vitro differentiation, CMG-ME cells were plated onto fibronectin-coated dishes and treated with 3 μmol/L of 5-azacytidine (Sigma Aldrich) for 24 hours.

Intra-BM transplantation of CMG cells

One-hundred thousand CMG cells transduced with MSCV-GFP or CMG-ME cells were transplanted into the right tibia of lethally irradiated C3H mice by intra-BM injection using a previously described method.[20] Two-hundred thousand whole BM cells separated from C3H mice also were injected into the recipient mice to serve as radioprotective cells. When the mice were killed, the engraftment of the CMG-ME cells and the CMG cells that were transduced with MSCV-GFP was confirmed by polymerase chain reaction (PCR) and enzyme immunohistochemistry, respectively.

PCR analysis

The presence of the transgene was detected by PCR. The following primers were designed against the EGFP cDNA (5′ primer: 5′-CCAGTTCAGCGTGTCCGGCG-3′; 3′ primer: 5′-GGGGTCTTTGCTCAGGGCGG-3′). The PCR conditions have been previously described.[17]

Statistics

All values are presented as the mean ± SEM. Statistical significance was evaluated using unpaired Student *t* tests for comparisons between 2 mean values. Multiple comparisons between more than 3 groups were performed using an ANOVA. A value of P less than .05 was considered significant.

Results

Single HSC progeny are not a major source of new cardiomyocytes after cytokine-enhanced post-MI repair

In a previous report, we demonstrated that a single-cell transplantation analysis using cells that had the strongest dye-efflux activity ("Tip"-SP cells) with a phenotype of CD34$^-$c-Kit$^+$Sca-1$^+$Lin$^-$ (CD34$^-$KSL-SP) exhibited nearly complete (~ 96%) level of hematopoietic engraftment activity.[15] To first examine the contribution of BM-derived HSCs to the regeneration of cardiomyocytes after MI, we transplanted either whole BM cells (w-BM) or single CD34$^-$KSL-SP cells from transgenic EGFP mice into irradiated mice, induced MI, treated the mice with G-CSF daily for 10 days to mobilize the BM cells to the heart, and then examined the hearts using histologic methods (Figure 1A). Eight weeks after transplantation, the mean percentages of EGFP$^+$ cells among the peripheral blood nucleated cells of the mice transplanted with w-BM and that of the mice transplanted with single CD34$^-$KSL-SP cells were 87% ± 3% (n = 10) and 63% ± 10% (n = 10), respectively. The peripheral blood nucleated cell counts (NCCs), measured 24 hours after the last injection of G-CSF, were significantly higher in the G-CSF–treated (G-CSF[+]) mice than in saline-injected (G-CSF[−]) mice (Figure 1B). No significant difference in the NCC of G-CSF(+) mice was observed between the w-BM group and the CD34$^-$KSL-SP group.

A histologic analysis performed 8 weeks after the MI showed a markedly higher degree of EGFP$^+$ cell infiltration into the infarcted area in G-CSF(+) mice than in G-CSF(−) mice (Figure 1C-F; Table 1). Among the G-CSF(+) mice, a greater degree of infiltration was seen in the w-BM group than in the CD34$^-$KSL-SP group. Nonspecific autofluorescence was distinguished as reported previously.[21] As a control, the same experiment was performed using wild C57BL/6 mice–derived BM cells as donor cells for BM transplantation. Figure 1G shows that no green fluorescence was observed in the infarct area of control mice, thus, G-CSF treatment–induced augmentation of green fluorescence was not due to nonspecific fluorescence. The presence of the EGFP gene in the infarcted area also was confirmed by PCR analysis (data not shown).

In the w-BM group, some of the EGFP$^+$ cells in the ischemic area expressed actinin and showed striations, suggesting that they

Table 1. Quantitative analysis of EGFP⁺ cells in infarcted area

Mice	EGFP⁺ cells	
	Total*	Actinin⁺
w-BM G-CSF (−)	8841	85
(n = 5)	(1478, 1757, 1515, 2348, 1743)	(18, 15, 9, 9, 14)
w-BM G-CSF (+)	119802	5403
(n = 5)	(25006, 19950, 28303, 17633, 28910)	(1016, 982, 1328, 921, 1156)
CD34⁻ KSL-SP G-CSF (−)	1224	0
(n = 5)	(254, 183, 210, 300, 277)	(0, 0, 0, 0, 0)
CD34⁻ KSL-SP G-CSF (+)	41779	3
(n = 5)	(8654, 7005, 9217, 9034, 7869)	(0, 0, 1, 0, 2)

Whole bone marrow cells (w-BM) or single CD34⁻ c-kit⁺Sca-1⁺ lineage⁻ side population (CD34⁻ KSL-SP) cells from the BM of EGFP mice were transplanted into lethally irradiated C57BL/6 mice. Myocardial infarction (MI) was induced 8 weeks later. Commencing 24 hours after induction of MI, a saline solution (G-CSF [−]) or G-CSF (G-CSF [+]) was injected into the mice for 10 consecutive days. Eight weeks after induction of MI, the mice were sacrificed, and the hearts were subjected to immunohistological analysis. The number of EGFP⁺ and EGFP⁺ actinin⁻ cells in the infarcted area was scored using 100 specimens per group of mice (20 samples from the mid-left ventricle per mouse).

*Total numbers of EGFP⁺ cells in the infarcted area.

were cardiomyocytes (Figure 1H-I; Table 1). Some EGFP⁺ cells also expressed sarcomeric myosin or cardiac troponin I (data not shown). Very few EGFP⁺ actinin⁻ cells were seen in the 2 CD34⁻KSL-SP groups (Figure 1J; Table 1), which was consistent with previous reports.[12,13] The marked increase in EGFP⁺ actinin⁺ cells in the w-BM groups cannot be explained simply by the superiority of hematopoietic chimerism in the w-BM group (87% ± 3% vs 63% ± 10%) if regenerated cardiomyocytes were derived from HSCs. Collectively, these results suggest that the major population of cells mobilized from the BM and active in the regeneration of cardiomyocytes was nonhematopoietic in origin.

HSCs have little potency to differentiate into a mesenchymal lineage

Next, we compared the nonhematopoietic BM cell populations of mice transplanted with single CD34⁻KSL-SP cells or w-BM cells from transgenic EGFP mice. We cultured the BM cells from both groups of mice (n = 5 per group) with a high chimerism (> 80%) of EGFP⁺ donor cells using fibronectin-coated, 96-well plates. After 14 days of culture, the adherent cells were stained with anti-GFP and anti-CD45, and the frequency of donor-derived nonhematopoietic cells was determined using 3 specimens from each mouse BM. A significant proportion of the adherent cells from the BM of the w-BM group was positive for EGFP (EGFP⁺CD45⁻ mononuclear cells = 22.38%).

On the other hand, most of the adherent cells from the BM of the CD34⁻KSL-SP group were negative for EGFP (EGFP⁺CD45⁻ mononuclear cells = 0.8%, $P < .001$). These adherent cells were further cultured in either adipocyte- or osteocyte-inducing conditions for another 14 days; 200 adipocytes and 200 osteocytes among the adherent cells of the CD34⁻KSL-SP group were counted, but no EGFP⁺ cells were found (data not shown). These results suggest that purified HSCs have very little potency to differentiate into a mesenchymal lineage, while MSCs are feasible candidates for the source of regenerated cardiomyocytes among nonhematopoietic BM cells.[6-10] Based on these results, we focused on the contribution of MSCs in w-BM in the regeneration of cardiomyocytes after MI.

Clonal MSC progeny contribute to the regeneration of cardiomyocytes after cytokine-enhanced post-MI repair

Unlike HSCc, MSCs are difficult to purify prospectively according to surface phenotypes. Therefore, to assess the contribution of BM-derived MSCs to the regeneration of cardiomyocytes after MI, we designed a series of experiments using cardiomyogenic (CMG) cells,[6] a clonally isolated cell line of MSCs (Figures 2A and 3A). CMG cells can differentiate into spontaneously beating cardiomyocytes in vitro after exposure to 5-azacytidine. Since cultured MSCs are known to lose their BM homing ability,[22] we first confirmed that the CMG cells, tagged by transfection with the MSCV-EGFP retrovirus vector,[16] could be engrafted into the recipients' BM (n = 5) by intra-BM injection,[20] rather than intravenous injection, and differentiate into multiple lineages in a manner similar to that of authentic MSCs (Figure 2A). We detected EGFP⁺ cells in the BM, most of which had differentiated into adipocytes and osteocytes (Figure 2B-F), and we also found a small number of cells residing among the stromal cells (Figure 2D, F, G). We detected EGFP⁺ cells in several other organs, although in very low numbers (4, 5, 0, 0, 0, and 0 EGFP⁺ cells per 100 specimens [20 specimens per mouse] in the liver, kidney, heart, brain, skeletal muscle, and spleen, respectively) (Figure 2H-I).

To detect cardiomyocytes derived from CMG cells with a higher sensitivity and specificity, cells transfected with a pMLC2v-EGFP plasmid encoding EGFP driven by the myosin light chain promoter (CMG-ME cells) were prepared by selection with G418 and then treated with 5-azacytidine. Ten days after treatment, 6% of the cells were positive for EGFP and negative for actinin but expressed GATA4 (Figure 3B-C). After 3 weeks, most of the EGFP⁺ cells became actinin positive and developed a rod-like appearance (Figure 3D-E); at 4 weeks, they exhibited spontaneous beating. These findings demonstrate that the CMG-ME cells that were committed to cardiomyocytes could be detected by the expression of EGFP in this system.

Uncommitted CMG-ME cells then were transplanted directly into the BM of lethally irradiated C3H/He (C3H) mice, MI was induced, and the mice were treated with G-CSF (Figure 3A). Eight weeks after induction of MI, the mice (n = 5) were killed, and PCR analysis confirmed the engraftment of CMG-ME cells in the BM of all recipients (Figure 3F). The myocardium of the 5 mice was analyzed using immunofluorescence, and a total of 1034 EGFP⁺ actinin⁺ cells in 100 samples (20 samples per mouse) were observed. The number of EGFP⁺ actinin⁺ cells from each group of 20 samples from each mouse was 253, 92, 135, 327, and 227. This result indicated that CMG-ME cells mobilized from the BM contributed to the regeneration of the myocardium after MI (Figure 3G-H). The presence of the EGFP gene in the infarcted area also was confirmed by PCR analysis (data not shown). Although the number of detected cells was

lower than that observed in mice transplanted with whole BM, CMG-derived cardiomyocytes were clearly visible in the ischemic myocardium. We did not detect EGFP$^+$ cells in any other organs such as liver, kidney, skeletal muscle, and BM (data not shown). These results suggested that the myosin light chain promoter restricted EGFP expression to cardiac tissue.

Discussion

Although BM-derived cells were reported to differentiate into cardiomyocytes after MI,[3-5] the identity of specific cell types involved has not been determined. There are 2 possibilities: first, BM-derived HSCs trans-differentiated into cardiomyocytes. Second, other cell types, such as MSCs, regenerated cardiomyocytes. To address this issue, we performed 2 independent clonal analyses to test which cell types contribute to cardiomyocyte regeneration. The results suggest that MSCs, but not HSCs, in BM play a major role in the regeneration of myocardial tissue after MI.

Purified HSCs and their progeny rarely contributed to the regeneration of cardiomyocytes, even with G-CSF treatment after single-cell transplantation following MI induction. On the other hand, w-BM transplantation resulted in marked increase of the donor-derived cardiomyocytes after MI and subsequent treatment with G-CSF. The results suggest that the repopulation of cardiomyocytes was achieved by nonhematopoietic cells in BM rather than HSCs and their progeny. In addition, we did not detect any EGFP$^+$ MSCs in the CD34$^-$KSL-SP group, while a precise analysis indicated that around 90% of the MSCs, assayed as fibroblastic colony-forming units (CFU-Fs), were derived from donor mice in the w-BM transplantation model when the recipient mice received more than 7 Gy of total body irradiation.[22] These results led us to focus on the nonhematopoietic population of MSCs in BM as a candidate for the donor-derived cardiomyocytes.

While HSCs can be purified prospectively according to their surface phenotypes, such purification is difficult to achieve for MSCs. Therefore, we used a cell line of MSCs to clonally identify the origin of BM-derived cardiomyocytes after MI. CMG cells, previously established from MSCs in the BM of C3H mice, can differentiate into spontaneously beating cells with a fetal ventricular cardiomyocyte phenotype in vitro after exposure to 5-azacytidine.[6] Since only a small fraction of these cells differentiate into cardiomyocytes and CMG cells were sporadically found in other organs after intra-BM injection (Figure 2H-I), we labeled the CMG cells to improve specific detection. Although the number of detected cells was smaller than that observed in mice that received transplants of whole BM, CMG-derived cardiomyocytes were clearly detected in the ischemic myocardium; these results are the first evidence that CMG cells can differentiate into cardiomyocytes in the cardiac niche without 5-azacytidine treatment. Most of the CMG cells that were transplanted directly into the BM differentiated into bone tissue (Figure 2D-E). This is most likely because insertion of the needle into the BM cavity stimulated osteogenesis[23]; such activity may account for the small number of CMG-derived cardiomyocytes. Systemic intravenous delivery of CMG may obviate this loss of CMG cells to osteogenesis and improve cardiomyocyte differentiation.[24] However, the intravenous delivery of cultured MSCs to BM is limited by either a defect in the homing ability of the cells[22] or the entrapment of the cells in the lungs.[25] A limitation of these experiments is that the CMG cell population isolated in vitro might not be a natural cell lineage. An important future experiment is to determine whether authentic MSCs purified from the BM can regenerate cardiomyocytes using the protocol outlined in Figure 3A.

Human MSCs were reported to mobilize into the systemic circulation as a result of G-CSF treatment.[26] The present study also shows that G-CSF treatment induces mobilization of MSCs from the BM into the systemic circulation leading to engraftment at peripheral organ sites. Matrix metalloproteinases and elastase, released mainly from granulocytes, are thought to be the major mediators of HSC mobilization induced by G-CSF.[27] The role of these factors in mediating the mobilization of MSC is unknown and provides an important avenue for future research. As G-CSF treatment following MI is reported to improve cardiac function and survival,[5] MSC mobilization may provide a new strategy for regenerative treatment. Furthermore, the data presented here support the concept that one function of MSC in BM is to contribute to the repair of injured tissue by being mobilizing to the site of injury and differentiating according to the niche.[25,26,28,29]

While this study focused on cardiomyocytes derived from BM, the reported improvement of infarcted tissue by G-CSF cannot be solely attributed to these cells. Most of the donor-derived cells in the infarcted area were actinin-negative fibroblastic cells and endothelial cells derived from HSCs. It is possible that these cells are f-macrophages[30] or are generated by fusion.[11] The role of these cells in remodeling is now under investigation. Neovascularization by endothelial progenitor cells (EPCs) mobilized from BM by G-CSF is also reported to contribute to an improved outcome.[27] In addition, EPC are reported to transdifferentiate into cardiomyocytes.[31] Adult cardiac stem cells in the heart[32,33] and multipotent adult progenitor cells[34] also may be affected by G-CSF. Therefore, the clinical significance of cardiomyocyte regeneration by BM-derived cells must take into account the role of different populations of cells in the regeneration process. The outcome of this research should be the development of novel cytokine and cell-based therapies for MI.

Acknowledgments

The authors thank Tadayuki Sato, Hideyuki Matsuzawa, and Takashi Yahata for their technical assistance.

References

1. Weissman, IL, Anderson DJ, Gage F. Stem and progenitor cells: origins, phenotypes, lineage commitments, and transdifferentiations. Ann Rev Cell Dev Biol. 2001;17:387-403.
2. Poulsom R, Alison MR, Forbes SJ, Wright NA. Adult stem cell plasticity. J Pathol. 2002;197:441-456.
3. Orlic D, Kajstura J, Chimenti S, et al. Bone marrow cells regenerate infarcted myocardium. Nature. 2001;410:701-705.
4. Jackson KA, Majka SM, Wang H, et al. Regeneration of ischemic cardiac muscle and vascular endothelium by adult stem cells. J Clin Invest. 2001;107:1395-1402.
5. Orlic D, Kajstura J, Chimenti S, et al. Mobilized bone marrow cells repair the infarcted heart, improving function and survival. Proc Natl Acad Sci U S A. 2001;98:10344-10349.
6. Makino S, Fukuda K, Miyoshi S, et al. Cardiomyocytes can be generated from marrow stromal cells in vitro. J Clin Invest. 1999;103:697-705.
7. Hakuno D, Fukuda K, Makino S, et al. Bone marrow–derived cardiomyocytes (CMG cell) expressed functionally active adrenergic and muscarinic receptors. Circulation. 2002;105:380-386.
8. Fukuda K. Development of regenerative cardiomyocytes from mesenchymal stem cells for cardiovascular tissue engineering. Artif Organs. 2001;25:183-193.
9. Toma C, Pittenger MF, Cahill KS, Byrne BJ, Kessler PD. Human mesenchymal stem cells differentiate to a cardiomyocyte phenotype in the adult murine heart. Circulation. 2002;105:93-98.

10. Tomita S, Li RK, Weisel RD, et al. Autologous transplantation of bone marrow cells improves damaged heart function. Circulation. 1999; 100(suppl II):247-256.
11. Alvarez-Dolado M, Pardal R, Garcia-Verdugo JM, et al. Fusion of bone-marrow–derived cells with Purkinje neurons, cardiomyocytes and hepatocytes. Nature. 2003;425:968-973.
12. Murry CE, Soonpaa MH, Reinecke H, et al. Haematopoietic stem cells do not transdifferentiate into cardiac myocytes in myocardial infarcts. Nature. 2004;428:664-668.
13. Balsam LB, Wagers AJ, Christensen JL, et al. Haematopoietic stem cells adopt mature haematopoietic fates in ischaemic myocardium. Nature. 2004;428:668-673.
14. Kawamoto S, Niwa H, Tashiro F, et al. A novel reporter mouse strain that expresses enhanced green fluorescent protein upon Cre-mediated recombination. FEBS Lett. 2000;470:263-268.
15. Matsuzaki Y, Kinjo K, Mulligan RC, Okano H. Unexpectedly efficient homing capacity of purified murine hematopoietic stem cells. Immunity. 2004; 20:87-93.
16. Hawley RG, Lieu FH, Fong AZ, Hawley TS. Versatile retroviral vectors for potential use in gene therapy. Gene Ther. 1994;1:136-138.
17. Oki M, Ando K, Hagihara M, et al. Efficient lentiviral transduction into human cord blood cd34(+) cells and differentiation into dendritic cells. Exp Hematol. 2001;29:1210-1217.
18. O'Brien TX, Lee KJ, Chien, KR. Positional specification of ventricular myosin light chain 2 expression in the primitive murine heart tube. Proc Natl Acad Sci U S A. 1993;90:5157-5161.
19. Henderson SA, Spencer M, Sen A, et al. Structure, organization, and expression of the rat cardiac myosin light chain-2 gene: identification of a 250-base pair fragment which confers cardiac-specific expression. J Biol Chem. 1989;264: 18142-18148.
20. Yahata T, Ando K, Sato T, et al. A highly sensitive strategy for scid-repopulating cell assay by direct injection of primitive human hematopoietic cells into NOD/SCID mice bone marrow. Blood. 2003; 101:2905-2913.
21. Jackson KA, Snyder DS, Goodell MA. Skeletal muscle fiber–specific green autofluorescence: potential for stem cell engraftment artifacts. Stem Cells. 2004;22:180-187.
22. Rombouts WJC, Ploemacher RE. Primary murine MSC show highly efficient homing to the bone marrow but lose homing ability following culture. Leukemia. 2003;17:160-170.
23. Gazit D, Karmish M, Holzman L, Bab I. Regenerating marrow induces systemic increase in osteo- and chondrogenesis. Endocrinology. 1990;126: 2607-2613.
24. Liechty KW, MacKenzie TC, Shaaban AF, et al. Human mesenchymal stem cells engraft and demonstrate site-specific differentiation after in utero transplantation in sheep. Nat Med. 2000;6: 1282-1286.
25. Barbash IM, Chouraqui P, Baron J, et al. Systemic delivery of bone marrow–derived mesenchymal stem cells to the infarcted myocardium: feasibility, cell migration, and body distribution. Circulation. 2003;108:863-868.
26. Kocher AA, Schuster MD, Szabolcs MJ, et al. Neovascularization of ischemic myocardium by human bone-marrow–derived angioblasts prevents cardiomyocyte apoptosis, reduces remodeling and improves cardiac function. Nat Med. 2001;7:430-436.
27. Lapidot T, Petit I. Current understanding of stem cell mobilization: the roles of chemokines, proteolytic enzymes, adhesion molecules, cytokines, and stromal cells. Exp Hematol. 2002;30:973-981.
28. Prockop DJ. Marrow stromal cells as stem cells for nonhematopoietic tissues. Science. 1997;276: 71-74.
29. Bittira B, Shum-Tim D, Al-Khaldi A, Chiu RCJ. Mobilization and homing of bone marrow stromal cells in myocardial infarction. Eur J Cardiothorac Surg. 2003;24:393-398.
30. Zhao Y, Glesne D, Huberman E. A human peripheral blood monocyte–derived subset acts as pluripotent stem cells. Proc Natl Acad Sci U S A. 2003;100:2426-2431.
31. Badorff C, Brandes RP, Popp R, et al. Transdifferentiation of blood-derived human adult endothelial progenitor cells into functionally active cardiomyocytes. Circulation. 2003;107:1024-1032.
32. Beltrami AP, Barlucchi L, Torella D, et al. Adult cardiac stem cells are multipotent and support myocardial regeneration. Cell. 2003;114:763-776.
33. Oh H, Bradfute SB, Gallardo TD, et al. Cardiac progenitor cells from adult myocardium: Homing, differentiation, and fusion after infarction. Proc Natl Acad Sci U S A. 2003;100:12313-12318.
34. Jiang Y, Jahagirdar BN, Reinhardt RL, et al. Pluripotency of mesenchymal stem cells derived from adult marrow. Nature. 2002;418:41-49.

THE JOURNAL OF BIOLOGICAL CHEMISTRY
Vol. 279, No. 48, Issue of November 26, pp. 50429–50436, 2004
Printed in U.S.A.

Down-regulation of p27^{Kip1} Promotes Cell Proliferation of Rat Neonatal Cardiomyocytes Induced by Nuclear Expression of Cyclin D1 and CDK4

EVIDENCE FOR IMPAIRED Skp2-DEPENDENT DEGRADATION OF p27 IN TERMINAL DIFFERENTIATION*

Received for publication, March 19, 2004, and in revised form, September 3, 2004
Published, JBC Papers in Press, September 13, 2004, DOI 10.1074/jbc.M403084200

Mimi Tamamori-Adachi‡§, Kentaro Hayashida‡§¶, Kiyoshi Nobori‡, Chie Omizu‡, Kazuhiko Yamada‡, Naoya Sakamoto‖, Takumi Kamura, Keiichi Fukuda¶, Satoshi Ogawa¶, Keiichi I. Nakayama**, and Shigetaka Kitajima‡ ‡‡**

*From the ‡Department of Biochemical Genetics, Medical Research Institute and Laboratory of Genome Structure and Regulation, School of Biomedical Science, the ‖Department of Gastroenterology and Hepatology, Tokyo Medical and Dental University, 1-5-45 Yushima, Bunkyo-ku, Tokyo, 113-8510, Japan, the ¶Cardiopulmonary Division, Department of Internal Medicine, Keio University School of Medicine, 35 Shinano-machi, Shinjyuku-ku, Tokyo 160-8582, Japan, and the **Department of Molecular and Cellular Biology, Medical Institute of Bioregulation, Kyushu University, 3-1-1, Maidashi, Higashi-ku, Fukuoka 812-8582, Japan*

Mammalian cardiomyocytes lose their capacity to proliferate during terminal differentiation. We have previously reported that the expression of nuclear localization signal-tagged cyclin D1 (D1NLS) and its partner cyclin-dependent kinase 4 (CDK4) induces proliferation of rat neonatal cardiomyocytes. Here we show that the D1NLS/CDK4 cells, after their entry into the cell cycle, accumulated cyclin-dependent kinase inhibitor p27 in the nuclei and decreased the cyclin-dependent kinase 2 (CDK2) activity, leading to early cell cycle arrest. Biochemical analysis demonstrated that Skp2-dependent p27 ubiquitylation was remarkably suppressed in cardiomyocytes, whereas Skp2, a component of Skp1-Cullin-F-box protein ubiquitin ligase, was more actively ubiquitylated compared with proliferating rat fibroblasts. Specific degradation of p27 by co-expressing Skp2 or p27 small interfering RNA caused an increase of CDK2 activity and overrode the limited cell cycle. These data altogether indicate that the impaired Skp2-dependent p27 degradation is causally related to the loss of proliferation in cardiomyocytes. This provides a novel insight in understanding the molecular mechanism by which mammalian cardiomyocytes cease to proliferate during terminal differentiation.

Terminal differentiation of highly specialized cells such as neural cells, cardiomyocytes, and pancreatic β cells is an important biological process that ensures their proper mass and function in higher organism. This process is accompanied with cell cycle arrest that is a hallmark of terminally differentiated cells. However, it is poorly understood how these cells cease to proliferate or more specifically whether their cell cycle can be reactivated. Mammalian cardiomyocytes irreversibly withdraw from the cell cycle soon after birth and lose the cell proliferative activity (1–4), although it has been shown that the adult heart contains a small population of cardiac progenitors that retain the proliferation capacity (5, 6). It is recently demonstrated that cardiac progenitor cells from embryonic or bone marrow stem cells are differentiated into functional cardiomyocytes when grafted in the damaged cardiac tissue (5). In addition to these, several approaches have been made to reactivate the cell cycle of terminally differentiated cardiomyocytes. For instance, adenoviral delivery of E2F allowed these cells to enter the cell cycle. However, this could not support cell proliferation but caused apoptotic cell death (7–9). This failure of cell proliferation may be largely because of our limited knowledge of the molecular events of cell cycle arrest underlying terminal differentiation of cardiomyocytes.

We have recently reported that the nuclear expression of cyclin D1 (D1NLS)[1]/cyclin-dependent kinase (CDK) 4 promoted the proliferation of rat neonatal cardiomyocytes in culture as well as adult rat heart *in situ* (10). Furthermore, there observed no induction of apoptotic cell death. This argues that the nuclear import of cyclin D1 is impaired in adult cardiac cells and these cells could be allowed to enter the cell cycle once this step is bypassed. This may illustrate one of the molecular features of adult cardiomyocytes that cease to grow after terminal differentiation. However, our knowledge is still limited regarding the molecular mechanism by which the proliferation of adult cardiomyocytes is suppressed or how it is reactivated. It is also unknown whether there is a cell cycle barrier other than the nuclear import of cyclin D1.

Progression of the mammalian cell cycle is regulated with a combination of positive and negative regulators (11). It is activated by a family of cyclins and CDKs. During the G_1 phase, cyclin D1 and other D-type cyclins accumulate in nuclei and assemble with their catalytic partners, CDK4 and CDK6. For example, the cyclin D1-CDK4 complex phosphorylates and in-

* This work was supported in part by a grant-in-aid for Scientific Research from the Ministry of Education, Science, Sports, Culture and Technology of Japan, the Japan Society for the Promotion of Science, a grant from the Japan Space Forum, and a grant from the Atsuko Ouchi Memorial Fund. The costs of publication of this article were defrayed in part by the payment of page charges. This article must therefore be hereby marked "*advertisement*" in accordance with 18 U.S.C. Section 1734 solely to indicate this fact.

§ Both authors contributed equally to this work.

‡‡ To whom correspondence should be addressed: Dept. of Biochemical Genetics, Medical Research Institute and Laboratory of Genome Structure and Regulation, School of Biomedical Science, Tokyo Medical and Dental University, 1-5-45, Yushima, Bunkyo-ku, Tokyo 113-8510, Japan. Tel.: 81-3-5803-5822; Fax: 81-3-5803-0248; E-mail: kita.bgen@mri.tmd.ac.jp.

[1] The abbreviations used are: D1NLS, nuclear localization signal-tagged cyclin D1; CDK, cyclin-dependent kinase; SCF, Skp1/Cul1/F-box; siRNA, small interfering RNA; APC/Ccdh1, anaphase-promoting complex/cyclosome and its activator Cdh1.

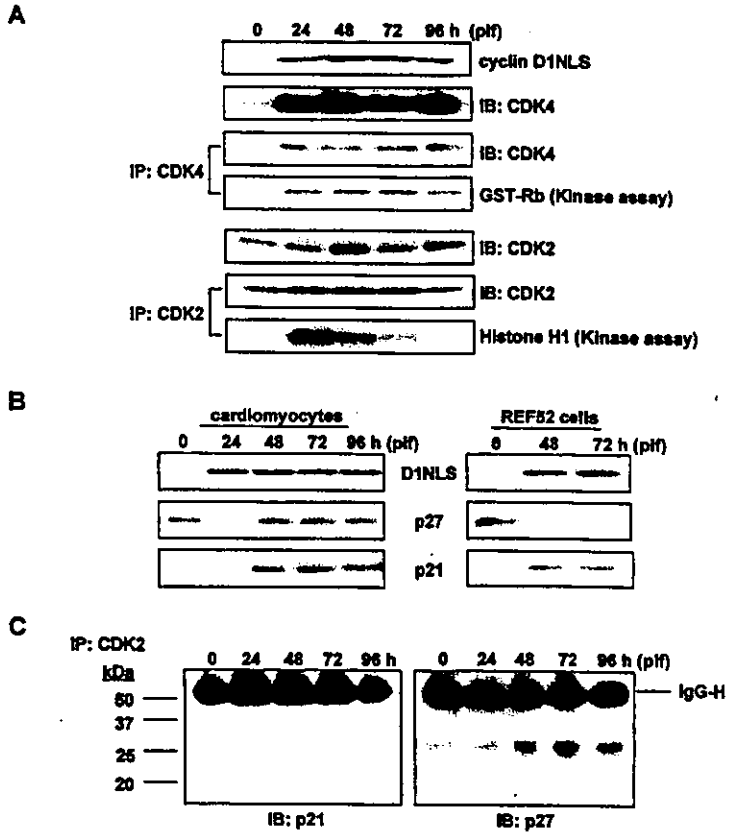

FIG. 1. **CDK2 activity was suppressed and p27 accumulated in cardiomyocytes after cell cycle entry by D1NLS/CDK4.** Rat neonatal cardiomyocytes were infected with a combination of AdD1NLS and AdCDK4 as described under "Experimental Procedures." *A*, at each time indicated, cell extracts were immunoprecipitated using anti-CDK4 and anti-CDK2 antibodies, and assayed for CDK4 and CDK2 activity, respectively. In *B*, the cell extract from the D1NLS/CDK4-infected cardiomyocytes or REF52 cells was subjected to Western blot and assayed for CDK inhibitors, p27 and p21. *C*, extracts of the D1NLS/CDK4 cardiomyocytes were immunoprecipitated with anti-CDK2 antibody and analyzed for p21 and p27 protein by Western blot analysis using anti-IgG heavy chain-specific antibody as the secondary antibody. *IB*, immunoblot.

activates the retinoblastoma protein (Rb) and sequesters CDK inhibitors, thereby promoting cell cycle progression through the G_1 to S phase. On the other hand, the CDK inhibitors, such as CIP/KIP family proteins, negatively regulate progression of the cell cycle by inhibiting the activity of cyclin-CDK complexes. The CIP/KIP family proteins, including p21 and p27, suppress the activities of cyclin A/CDK2 and cyclin E/CDK2, respectively, and mediate the exit from the cell cycle.

The level of p27 increases in quiescent non-proliferating cells and decreases on entry into the cell cycle and is controlled by the rate of degradation in both cytoplasm and nuclei. The degradation of p27 in cytoplasm is associated with the transition of cells from the G_0 to G_1 phase, whereas nuclear degradation occurs during S and G_2 phases. In the latter, p27 is phosphorylated at threonine 187 and recruited to the F-box protein Skp2 of the SCF^{Skp2} complex. This is followed by multiple ubiquitylation and degradation through the 26 S proteasome. Among this cascade reaction, the recognition of p27 by Skp2 is specific and plays a central role in p27 degradation. Therefore, p27 degradation is essential for cells to undergo cell cycle progression (12–19). In the developing heart, p27 is reported to accumulate as it loses the cell growth capacity in the late stage of embryo and after birth (20). Furthermore, mice deficient for p27 sustained cell growth capacity after birth (21). These findings may suggest a role of p27 in the terminal differentiation of cardiomyocytes.

In the present study, we examined the cell cycle progression of rat neonatal cardiomyocytes that were forced to enter the cell cycle by nuclear expression of D1NLS and its partner CDK4 (10). It was shown that D1NLS/CDK4 cardiac cells ceased to proliferate after only one or two cell cycles and accumulated the CDK inhibitor p27 in the nuclei. The *in vitro* p27 ubiquitylation was remarkably suppressed in cardiomyocytes, whereas that of Skp2 was up-regulated. We further showed that knockdown of p27 or overexpression of Skp2 specifically degraded p27 and accelerated proliferation of D1NLS/CDK4 cardiomyocytes.

EXPERIMENTAL PROCEDURES

Reagents—Antibodies used in this study were as follow: mouse monoclonal anti-cyclin D1 (Ab-3, Oncogene Science), anti-sarcomeric actin (M0874, DAKO), anti-proliferating cell nuclear antigen (sc-056), and rabbit polyclonal anti-p21 (sc-6246), anti-p27 (sc-528), anti-Skp2 p45 (sc-7164), anti-CDK4 (sc-260), and anti-CDK2 (sc-163) from Santa Cruz Biotechnology, Santa Cruz, CA. Other biochemicals used were reagent grade.

Cell Culture—Rat neonatal cardiomyocytes were isolated and cultured as previously described (10, 22). Heart ventricles were isolated from 3-day-old postnatal Sprague-Dawley rats, trisected, and then digested 4 times with 1 mg/ml collagenase type II (Worthington) in Ads buffer (20 mM Hepes-KOH, pH 7.35, 116 mM NaCl, 5.4 mM KCl, 1 mM NaH_2PO_4, 0.8 mM $MgSO_4$, and 5 mM glucose) at 37 °C for 20 min. The dispersed cells were washed once by Ads buffer and then purified by centrifugation through a discontinuous Percoll gradient of 1.050, 1.060, and 1.082 g/ml, respectively. The cardiac cells at the interface between 1.060 and 1.082 g/ml were collected and plated on a 60-mm dish ($2–3 \times 10^6$ cells) or 25-mm collagen-coated coverslips ($2–3 \times 10^5$ cells) in minimum essential medium supplemented with 5% calf serum, 100 units/ml penicillin, and 100 μg/ml streptomycin. Cardiomyocytes were cultured at 37 °C for 24 h in humidified air with 5% carbon dioxide, after which the medium was changed to serum-free minimal essential medium and further incubated for another 24 h. The purity of cardiomyocytes was determined by immunostaining with anti-sarcomeric actin antibody and over 95% of cells were positive for sarcomeric actin. Rat fibroblast REF52 cells were cultured in Dulbecco's modified Eagle's medium (Sigma) containing 10% fetal calf serum as reported (10). Use of neonatal rats in this study was approved by the Institutional Animal Care and Use Committee of our university.

Adenoviruses and Their Gene Transfer—Adenoviruses for expressing nuclear localization signal-tagged cyclin D1 (Ad-D1NLS), CDK4 (Ad-CDK4), and Skp2 (Ad-Skp2) were as described (10, 23). Viruses were propagated in 293 cells, and the virus stocks were prepared as described (10, 22). Virus titer was determined by an indirect immunofluorescent

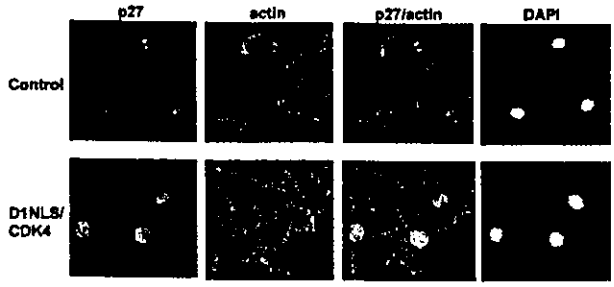

FIG. 2. **p27 accumulated in the nuclei of cardiomyocytes after cell cycle entry by D1NLS/CDK4.** Control untreated and D1NLS/CDK4 cells at 48 h post-infection were fixed and stained for p27 (*green*) and sarcomeric actin (*red*) with anti-p27 and anti-sarcomeric actin antibodies, respectively, as described under "Experimental Procedures." Cell nuclei (*white*) were also stained with 4′,6-diamidino-2-phenylindole (*DAPI*).

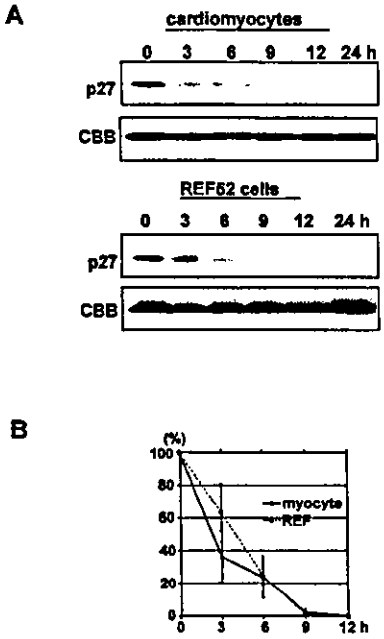

FIG. 3. **Serum-induced degradation of p27 in cardiomyocytes was not different from REF52 cells.** *A*, cardiomyocytes and REF52 cells were serum-starved for 48 h and then treated with serum (10% fetal bovine serum). At each time after adding the serum, cell extract (20 μg) was assayed for p27 by Western blot analysis. *Lower panels* show the Coomassie Brilliant Blue (*CBB*) staining as the control for protein loading. In *B*, the amount of p27 protein was quantitated by densitometric measurement and expressed as percent of that at time 0. Results represent the mean ± S.E. three independent experiments.

assay using anti-72K antibody. Cardiomyocytes were infected at the indicated multiplicity of infection in serum-free minimal essential medium for 60 min with brief agitation every 15 min, and then the medium was replaced with culture medium.

Construction of Adenovirus Vector Encoding p27 SiRNA—Oligonucleotides for expressing stem-loop RNAs that target three different regions of rat *p27* were ligated with human U6 promoter and the resulting transcription unit of the U6 promoter was subcloned into the SwaI site of the E1-deleted region of cassette cosmid vector pAxcw (Adenovirus Expression Vector Kit, TaKaRa BIO). Adenoviral vector was then prepared as in the protocol from Takaka. Oligonucleotide sequences used were: 5′-CACCGGTAGGAGGTTCTTCTTCAACGTGTGCTGTCCGTTGAAGAAGAATCTTCTGCCTTTTT-3′ and 5′-GCATAAAAAGGCAGAAGATTCTTCTTCAACGGACAGCACACGTTGAAGAAGAACCTCCTACC-3′ (#1) for the p27 amino acid region from 830 to 848, 5′-CACCAGTGTAAGTGGAGTTTCGAACGTGTGCTGTCCGTTCGAAATTCCACTTGCGCTTTTTT-3′ and 5′-GCATAAAAAAGCGCAAGTGGAATTTCGAACGGACAGCACACGTTCGAAACTCCACTTACACT-3′ (#4) from 532 to 550, or 5′-CACCGTGGGAGTGTTTAATGGGA-

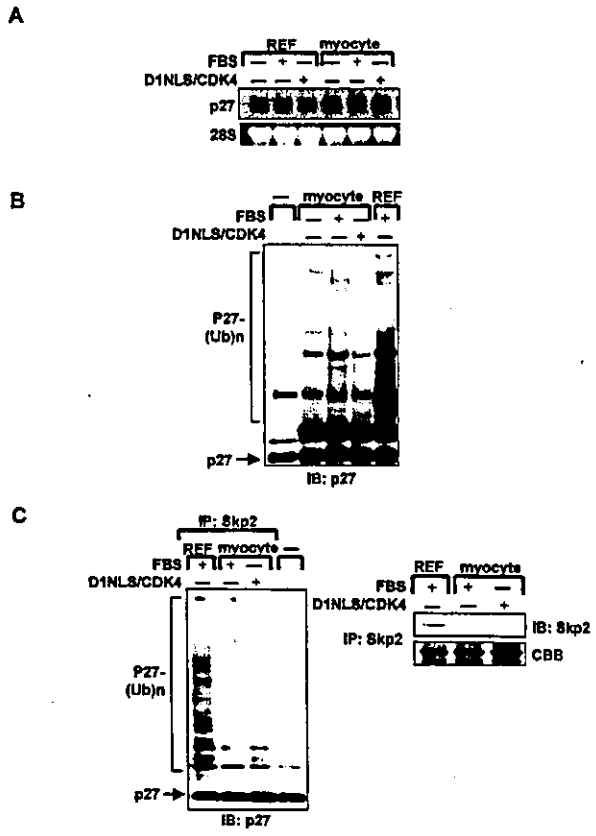

FIG. 4. **Cardiomyocytes showed the impaired Skp2-dependent degradation of p27.** *A*, total RNA (10 μg) from the control, serum, or D1NLS/CDK4-treated cardiomyocytes and REF52 cells was analyzed for p27 mRNA by Northern blot analysis as described under "Experimental Procedures." *B*, equal amounts of cell extract (50 μg of protein) treated as in *A* were assayed for the *in vitro* p27 ubiquitylation activity as described under "Experimental Procedures." *C*, cell extracts (50 μg of protein) from cells treated as in *B* were immunoprecipitated with anti-Skp2 antibody and the resulting complexes were assayed for the Skp2 protein (*right panel*) and the *in vitro* p27 ubiquitylation activity (*left panel*), respectively. *CBB*, Coomassie Brilliant Blue; *FBS*, fetal bovine serum.

ACGTGTGCTGTCCGTTCCCGTTAGACACTCTCACTTTTT-3′ and 5′-GCATAAAAAGTGAGAGTGTCTAACGGGAACGGACAGCACACGTTCCCATTAAACACTCCCAC-3′ (#6) from 372 to 390, respectively. Adenovirus vector encoding siRNA for hepatitis C viral protein (siRNA331) was as described (24) and employed as control.

Whole Cell Extract Preparation and Western Blot Analysis—Cardiomyocytes (2×10^6 cells) treated as indicated were washed in phosphate-buffered saline, resuspended in 50 μl of lysis buffer (50 mM Hepes-KOH, pH 7.6, 150 mM NaCl, 1% Tween 20, 10 mM glycerophosphate, 2.5 mM EGTA, 1 mM EDTA, 0.1 mM phenylmethylsulfonyl fluoride, 10 μg/ml each leupeptin and aprotinin, 0.1 mM sodium vanadate, 1 mM NaF, and 10% glycerol), and incubated on ice for 30 min. After centrifugation at 12,000 rpm for 10 min, whole cell extract was obtained. The amount of protein was measured with the Lowry method using bovine serum albumin as standard. Whole cell extracts (usually 20 μg of protein) were separated by SDS-PAGE, transferred onto an Immobilon-P membrane (Millipore), and subjected to Western blot using the protocol of the ECL kit (Amersham Biosciences) as described (20).

Immunoprecipitation and Kinase Assays—Whole cell extracts (50 μg of protein) were immunoprecipitated with anti-CDK4 (0.4 μg) or anti-CDK2 antibody (0.4 μg) followed by Western blot with the indicated antibody, and bands were detected using monoclonal anti-rabbit IgG (γ-chain specific) peroxidase-conjugated secondary antibody (Sigma). To assay CDK4 and CDK2 kinase activity, the immunoprecipitated complexes were incubated with glutathione *S*-transferase-Rb and histone H1, respectively, as substrates as described (10, 22).

RNA Isolation and Northern Blot Analysis—Total RNA was isolated by the acid-guanidium method using Isogen (Nippon Gene, Japan),

fractionated on a formaldehyde/agarose gel, transferred to a Hybond-N membrane, and hybridized to random-primed cDNA probes for the mouse *p27* and *skp2* genes as described (22). The membrane was exposed and analyzed with a Bas 2500 Bioimage analyzer (Fujifilm Co., Tokyo, Japan). DNA fragments (100 ng) for these cDNAs were radiolabeled with 50 μCi of [α-^{32}P]dCTP (6000 Ci/mmol, Amersham Biosciences) using a random primer labeling kit from Takara and used as probe for RNA preparation and Northern blot analysis.

In Vitro Ubiquitylation Assay—Cells were treated in lysis buffer (20 mM Hepes-KOH, 0.42 M NaCl, 1.5 mM $MgCl_2$, 0.2 mM EDTA, 0.5% Nonidet P-40, 0.1 mM phenylmethylsulfonyl fluoride, 10 μg/ml each leupeptin and aprotinin, and 25% glycerol) on ice for 30 min, and cell debris was removed by centrifugation at 15,000 rpm for 20 min. Cell extract (50 μg of protein) was incubated with substrates in 15 μl of buffer of 40 mM Hepes-NaOH (pH 7.9), 60 mM potassium acetate, 2 mM dithiothreitol, 5 mM $MgCl_2$, 0.5 mM EDTA, 10% glycerol, and 1.5 mM ATP containing 50 ng of Uba1, 100 ng of UbcH5A, 3 μg of glutathione *S*-transferase-ubiquitin. After incubating at 26 °C for 30 min, reaction products were separated by SDS-PAGE and analyzed by Western blot with the indicated antibody. As substrates, FLAG-p27 or -Skp2 were prepared using 1 μg of pcDNA3Flag-p27 or pcDNA3Flag-skp2 (23) and 25 μl of rabbit reticulocyte lysate (TNT kit from Promega) according to its protocol. The *in vitro* p27 ubiquitylation activity was also assayed after immunoprecipitation of cell extracts with 0.4 μg of anti-Skp2 antibody.

Immunocytological Study and Cell Cycle Analysis—To examine the expression of p27 in cardiomyocytes, cells grown on glass coverslips were fixed in 70% ethanol, double-stained with anti-p27 and anti-sarcomeric actin antibodies, and visualized using fluorescent tyramide reagent according to the manufacturer's protocols (TSA-direct NEL-701, PerkinElmer Life Sciences, Inc.). Confocal images were obtained using the laser-scanning confocal image system (LSM510, Zeiss). For cell cycle analysis, cells were stained with anti-sarcomeric actin and anti-mouse antibodies conjugated with fluorescein isothiocyanate (23799, Polysciences), followed by treatment with propidium iodide (50 μg/ml) and RNase A (500 μg/ml). The DNA content of cells positive for sarcomeric actin was analyzed using a laser scanning cytometer (LSC 101, Olympus).

Statistical Analysis—Quantitative data were expressed as mean ± S.E. Statistical analysis was performed with the Student's *t* test.

RESULTS

CDK2 Activity Was Suppressed and the Cell Cycle Inhibitor p27 Accumulated in the Nuclei of Cardiomyocytes after Cell Cycle Entry by D1NLS/CDK4—We have previously shown that D1NLS/CDK4 expression allowed the cardiomyocytes to enter the cell cycle (10). However, the proliferation of these cells was limited to approximately one or two cycles. To understand the mechanism by which the cells cease to proliferate, we first assayed the activity of G_1 cyclin kinase, CDK4 and CDK2. As shown in Fig. 1*A*, the CDK4 activity was up-regulated at 24 h post-infection of D1NLS/CDK4, and remained active for at least 96 h. The CDK2 activity was also activated at 24 h, but suppressed again at 48 h, whereas the amount of CDK2 was not significantly affected. We, therefore, examined the expression of CDK2 inhibitors, p27 and p21. Fig 1*B* showed that p27 was accumulated in the serum-starved non-proliferating cardiomyocytes. When these cells were allowed to enter the cell cycle by D1NLS/CDK4, the p27 protein was rapidly degraded within 24 h. However, it accumulated again at 48 h, at which time CDK2 was inhibited (Fig. 1*A*). In REF52 fibroblasts, p27 was also rapidly degraded after entering the cell cycle by D1NLS/CDK4, but no accumulation was observed for at least 72 h. The expression of p21 was significantly suppressed in serum-starved cardiomyocytes and REF52 cells, but up-regulated at 48 h after the cell cycle entry. In Fig. 1*C*, immunoprecipitaion of the cardiomyocyte extract was performed using anti-CDK2 antibody. Results showed that p27 was little associated with CDK2 in the serum-starved cells, but the higher amount of p27 was detected in the CDK2 complex at 48–96 h. In contrast, appreciable amounts of p21 were not detected in the CDK2 complex. It was further noted that the expression of p57 and p53, other cell cycle inhibitors, was not significantly altered in D1NLS/CDK4 cells of this study (data not shown).

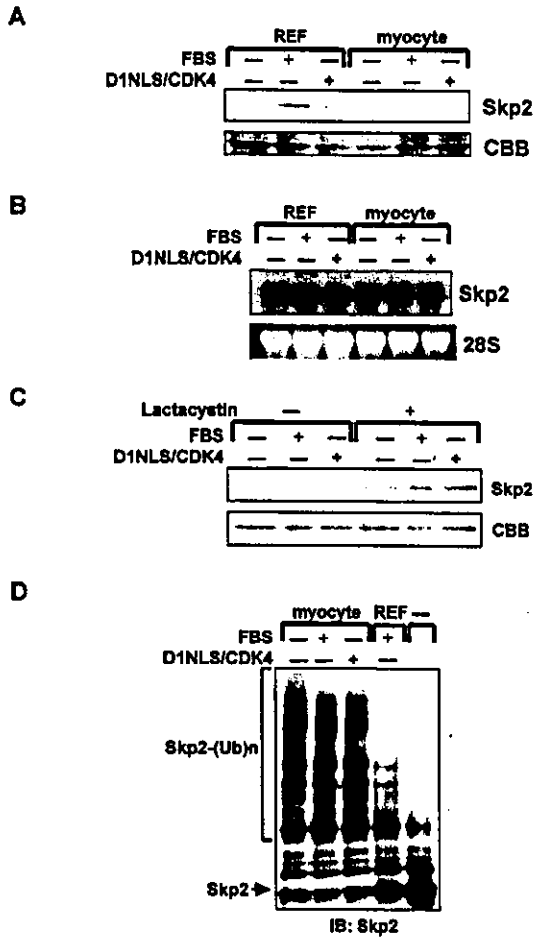

FIG. 5. **Down-regulation of Skp2 was inversely correlated to the *in vitro* Skp2 ubiquitylation activity in cardiomyocytes.** *A*, cardiomyocytes and REF52 cells were treated with serum (10% FBS) or D1NLS/CDK4 for 48 h, and their cell extracts (20 μg of protein) were assayed for Skp2 protein by Western blot analysis. *B*, cardiomyocytes and REF52 cells were treated as in *A*, and their total RNA (10 μg) was analyzed for Skp2 mRNA by Northern blot. *C*, cells were treated as in *A* in the presence or absence of 20 μM lactacystin, and their cell extracts were assayed for Skp2 protein by Western blot analysis. *Lower panels* show the Coomassie Brilliant Blue (*CBB*) staining as control for protein loading. *D*, cell extracts (50 μg of protein) were assayed for the *in vitro* Skp2 ubiquitylation activity as described under "Experimental Procedures." *IB*, immunoblot.

Next, the immunocytological study of p27 expression was performed. As shown in Fig. 2, p27 accumulated significantly in the nuclei of D1NLS/CDK4 cells, whereas its expression was little detected in control cells. These data altogether indicated that the p27 protein was degraded after initiation of cell cycle, but was accumulated again in the nuclei during cell cycle progression of cardiomyocytes.

Serum-induced Degradation of p27 in Cardiomyocytes Was Not Different from REF52 Cells—The protein level of p27 is predominantly controlled by the rate of degradation through the proteasome-dependent pathway. This degradation is mediated by the Skp2-independent ubiquitin ligase in the cytoplasm at G_0 to G_1 transition and by the Skp2-dependent ligase in the nuclei at S to G_2 phase, respectively (12, 17–19). In Fig. 3*A*, p27 accumulated when the cardiomyocytes and REF52 cells were serum-starved. We stimulated these cells with serum and the degradation of p27 was determined by Western blot analysis. Results showed that p27 was degraded in both cell types with

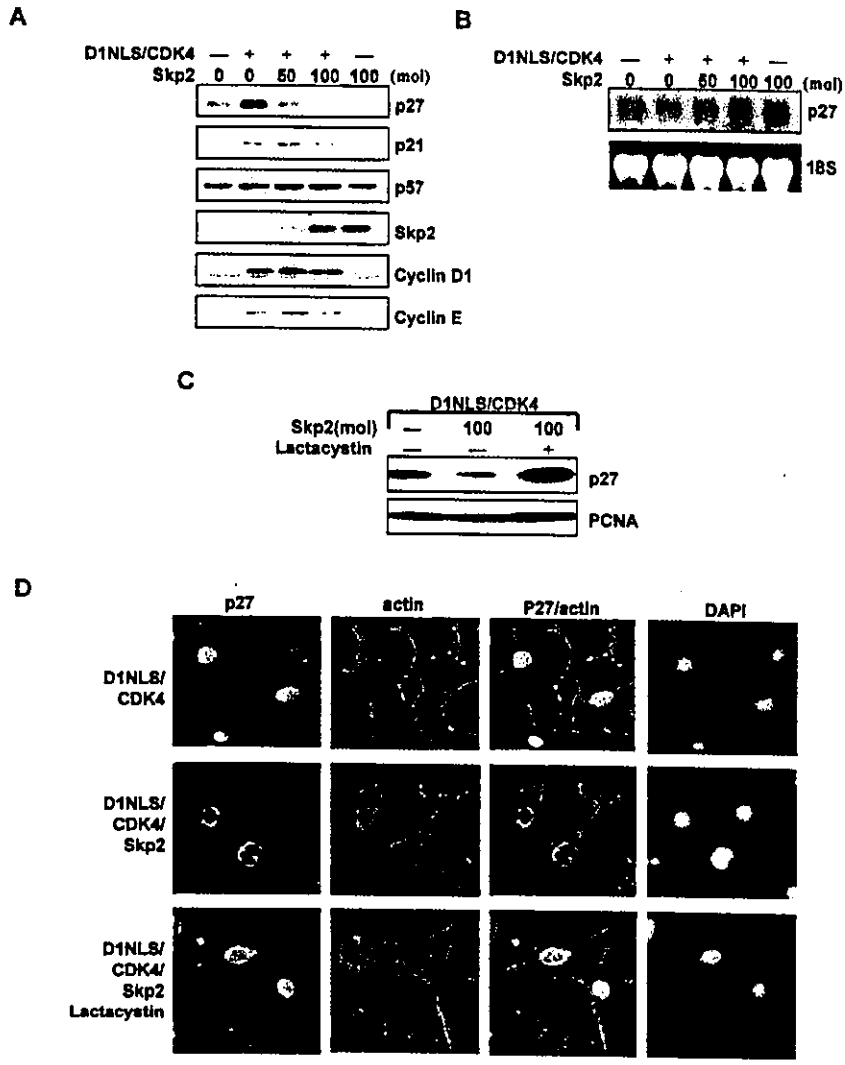

FIG. 6. **Skp2 expression caused a specific degradation of p27 in nuclei of D1NLS/CDK4 cardiomyocytes.** *A*, cardiomyocytes were infected with a combination of AdD1NLS/AdCDK4 and an increasing multiplicity of infection of Ad-Skp2. At 48 h post-infection, cell extracts (20 μg of protein) were prepared and assayed for various cell cycle regulators by Western blot analysis. *B*, total RNA (10 μg) was assayed for p27 mRNA as described in the legend to Fig. 3*A*. *C*, cardiomyocytes were treated as in *A* in the presence or absence of 20 μM lactacystin, and their extract (20 μg of protein) was assayed for p27 protein. Proliferating cell nuclear antigen (*PCNA*) was shown as a loading control. *D*, D1NLS/CDK4 and D1NLS/CDK4/Skp2 cardiomyocytes with or without 20 μM lactacystin treatment were immunostained for p27 with anti-p27 antibody. Sarcomeric actin and cell nuclei were also stained with anti-sarcomeric actin antibody and 4',6-diamidino-2-phenylindole (*DAPI*), respectively (*green*, p27; *red*, sarcomeric-actin; *white*, DAPI).

apparently similar kinetics (Fig. 3*B*). This strongly indicates that there is no apparent difference of p27 degradation between the cardiomyocytes and proliferating REF52 cells during their transition from G_0 to G_1 phase, although cardiac cells are not allowed to enter the cell cycle by serum treatment.

Skp2-dependent Degradation of p27 Was Suppressed in Cardiomyocytes—We next examined the p27 expression of cardiomyocytes after their entry into the cell cycle by D1NLS/CDK4 expression. The p27 mRNA level in cardiomyocytes was comparable with that of REF52 cells and unaltered by serum treatment or expression of D1NLS/CDK4 (Fig. 4*A*). We next examined p27 degradation by assaying the *in vitro* ubiquitylation activity. Fig. 4*B* showed that the p27 protein was highly ubiquitylated and migrated as a multiubiquitylated form when assayed using cell extract from REF52 cells. In contrast, the extracts from the control, serum-stimulated or D1NLS/CDK4-infected cardiomyocytes exhibited the lower activity compared with REF52 cells. We next examined the Skp2-dependent degradation of p27 after immunoprecipitating the Skp2-ligase complex. As shown in Fig. 4*C*, *left panel*, cardiomyocytes contained only marginal activity of p27 ubiquitylation, whereas REF52 cells exhibited significant activity. Under this condition, the complex from REF52 cells contained the higher amount of Skp2 protein than the cardiomyocytes (Fig. 4*C*, *right panel*). From these data, it is indicated that cardiomyocytes have much lower activity of Skp2-dependent p27 degradation than the growing REF52 cells.

Skp2 Protein Was Down-regulated through Its Accelerated Degradation in Cardiomyocytes—The data above strongly suggested that the impaired degradation of p27 by Skp2 might cause p27 accumulation during cell cycle progression of cardiomyocytes. We, therefore, examined the expression of Skp2 in cardiomyocytes. As shown in Fig. 5*A*, Skp2 protein was detected in the serum-starved REF52 cells, and it was induced after treatment with serum or D1NLS/CDK4. In cardiomyocytes, however, Skp2 expression was hardly detected or significantly suppressed in the serum-starved cardiac cells, and no significant induction was observed by serum or D1NLS/CDK4. Northern blot analysis revealed that apparently similar amounts of Skp2 mRNA was expressed in both cell types under these conditions (Fig. 5*B*). When these cardiomyocytes were treated with lactacystin, a proteasome inhibitor, Skp2 protein was remarkably stabilized (Fig. 5*C*), indicating that Skp2 protein was expressed but actively degraded in cardiomyocytes. Therefore, we further measured the *in vitro* ubiquitylation activity of Skp2 protein. Fig. 5*D* revealed that Skp2 protein was actively ubiquitylated and migrated as the multiubiquitylated products when assayed using extracts from cardiomyo-

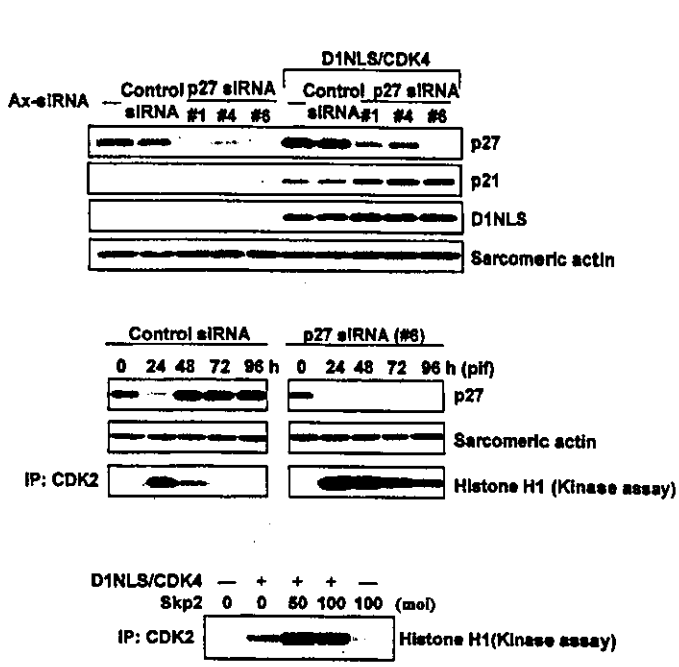

FIG. 7. **Specific down-regulation of p27 by siRNA or Skp2 abrogated early suppression of CDK2 activity in D1NLS/CDK4 cells.** *A*, cardiomyocytes were untreated or infected with a combination of AdD1NLS/AdCDK4 and adenovirus vectors encoding p27 siRNA 1, 4, 6, or hepatitis C viral protein (control). At 48 h post-infection, cell extracts (20 μg of protein) were prepared and assayed for p27, p21, and cyclin D1 by Western blot analysis. Sarcomeric actin was shown as control for protein loading. *B*, cells were infected with a combination of AdD1NLS/AdCDK4 and virus vector for control siRNA or p27 siRNA (*#6*). At the indicated time, cell extracts (20 μg) were assayed for p27 and CDK2 kinase (*Histone H1 kinase*) activity as described under "Experimental Procedures." *C*, cells were infected with a combination of AdD1NLS/AdCDK4 and an increasing multiplicity of infection of AdSkp2, and after 48 h, CDK2 activity was assayed as in *B*.

cytes, and this activity appeared not to be affected by serum or D1NLS/CDK4 treatment. In contrast, the activity was significantly suppressed in growing REF52 cells. This demonstrated that Skp2 degradation was highly activated in cardiomyoctes, and this was inversely correlated to the Skp2-dependent p27 degradation (Fig. 4*C*). From these results, it is indicated that the Skp2 protein is actively degraded in cardiomyocytes, possibly because of their increased Skp2 ubiquitylation, and this may in turn lead to the accumulation of the p27 protein.

Overexpression of Skp2 Caused Specific Degradation of p27—We next examined whether the down-regulation of Skp2 protein is functionally linked to accumulation of p27 in D1NLS/CDK4 cardiomyocytes. For this purpose, the Skp2 protein was overexpressed using the adenovirus-mediated gene transfer. As shown in Fig. 6*A*, the expression of Skp2 caused the significant degradation of p27 in D1NLS/CDK4 cells. In contrast, p21, p57, and cyclin D1 and E were only marginally affected. The p27 mRNA level was only slightly induced by Skp2 expression (Fig. 6*B*). Furthermore, the decrease of p27 by Skp2 expression was abrogated by lactacystin treatment (Fig. 6*C*), indicating that down-regulation of the p27 protein was specifically mediated by the Skp2-dependent degradation. Immunocytological study revealed that the accumulation of the p27 protein in the nuclei of D1NLS/CDK4 cardiomyocytes was significantly suppressed by Skp2 expression, and this suppression was inhibited by lactacystin treatment (Fig. 6*D*). These data altogether indicated that Skp2 enhanced the specific degradation of p27 in the nuclei of D1NLS/CDK4 cardiomyocytes through a proteasome-dependent pathway.

Down-regulation of p27 by siRNA or Skp2 Stimulated the CDK2 Activity and Overrode the Limited Cell Cycle Progression of D1NLS/CDK4 Cardiomyocytes—We further addressed whether the accumulation of p27 had a causal effect on the early cell cycle arrest of D1NLS/CDK4-infected cardiomyocytes. For this purpose, we employed a loss-of-function approach by an RNA interference-mediated gene knockdown. As shown in Fig. 7*A*, three vectors expressing different p27 siRNAs specifically caused the knockdown of p27 protein in both control and D1NLS/CDK4 cells, whereas they showed no inhibition of another CDK inhibitor p21. Next, we measured the p27 protein and CDK2 activity in D1NLS/CDK4 cells expressing these siRNAs. Fig. 7*B* showed that the suppression of CDK2 activity was totally abrogated when the re-accumulation of p27 was knocked down by p27 siRNA. By contrast, in cells expressing control siRNA, p27 was re-accumulated and CDK2 activity was suppressed as in D1NLS/CDK4 cells (compare with Fig. 1). The p27 degradation by Skp2 also prevented the suppression of CDK2 activity in D1NLS/CDK4 cells (Fig. 7*C*). These data strongly indicated that p27 played a major role in suppressing CDK2 activity in D1NLS/CDK4 cells.

Based on these results, we next measured cell cycle progression and proliferation by p27 siRNA or Skp2. Fig. 8*A* showed that a higher proportion of the D1NLS/CDK4/p27 siRNA or D1NLS/CDK4/Skp2 cells progressed to S/G_2M phase much faster than the D1NLS/CDK4 cells. Furthermore, these cells still retained the higher proportion of S/G_2/M cells at 192 h post-infection, compared with control D1NLS/CDK4 cells. When the cell number was counted, it was shown that p27 siRNA or Skp2 further promoted the proliferation of D1NLS/CDK4 cells (Fig. 8*B*). The apparent doubling time of cell proliferation was 64, 63.6, and 84 h for the D1NLS/CDK4/p27 siRNA, D1NLS/CDK4/Skp2, and D1NLS/CDK4 cells, respectively. By contrast, p27 siRNA or Skp2 expression alone had no significant effect. Therefore, it is indicated that down-regulation of p27 enhanced further stimulation of CDK2 activity and subsequent cell cycle progression of D1NLS/CDK4 cells.

DISCUSSION

In the present study, we demonstrated that the accumulation of CDK inhibitor p27 was a strong barrier of cell cycle in terminally differentiated cardiomyocytes, and this was caused, at least in part, by the impaired Skp2-dependent p27 degradation in the nuclei of cells.

p27 is degraded at least in two phases of the cell cycle. When cells transit from the G_0 to G_1 phase in response to growth stimuli such as serum, p27 is degraded in the cytoplasm by the Skp2-independent pathway. On the other hand, in proliferating cells, p27 is degraded in the nuclei during S and G_2 phase by a Skp2-dependent pathway (17, 19). The impaired Skp2-dependent nuclear degradation of p27 in cardiomyocytes is sup-

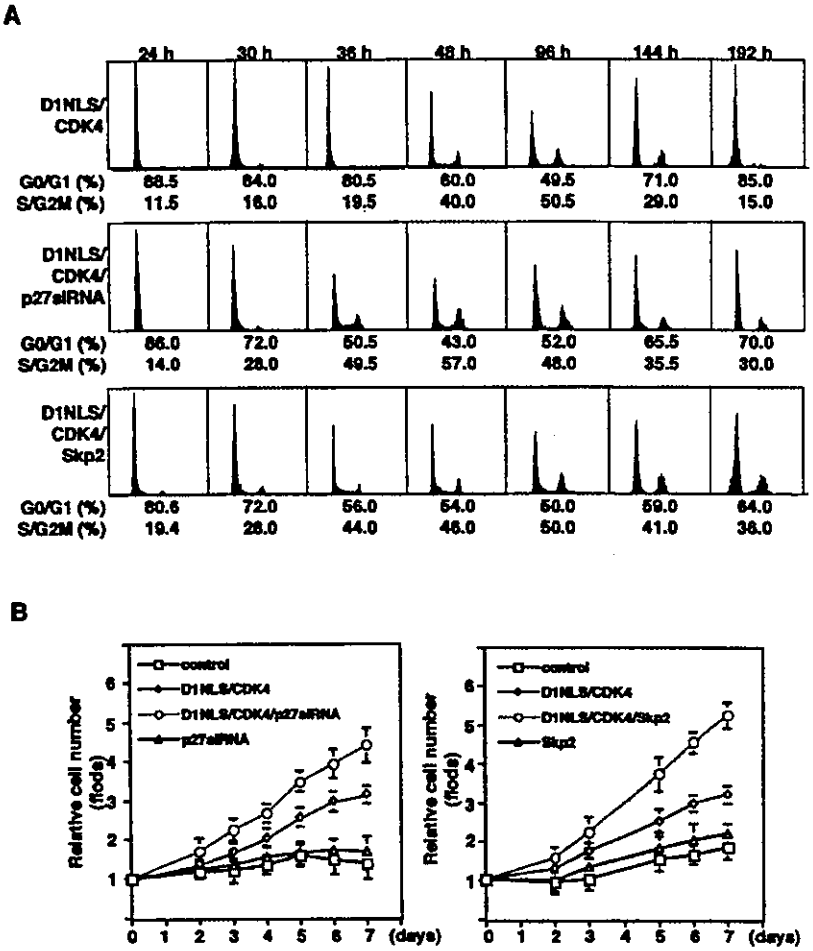

FIG. 8. **p27 down-regulation by siRNA or Skp2 promoted proliferation of D1NLS/CDK4 cardiomyocytes.** *A*, cells were infected with a combination of AdD1NLS/AdCDK4 along with Adp27 siRNA (#6) or AdSkp2. At each time indicated, cells were harvested and subjected to laser scanning cytometer analysis as described under "Experimental Procedures." *B*, cardiomyocytes were untreated or infected with a combination of AdD1NLS, AdCDK4, Adp27siRNA (#6), or AdSkp2 as indicated and cultured. Cell number was counted on the indicated day after infection, and the relative cell proliferation was expressed as mean ± S.E. of three independent experiments.

ported by the following findings, (i) *in vitro* p27 ubiquitylation activity of cell extracts or the Skp2 immunocomplex was remarkably suppressed in cardiomyocytes compared with proliferating REF52 fibroblasts (Fig. 4, *B* and *C*); (ii) p27 accumulation was observed in the nuclei of D1NLS cells (Fig. 2); (iii) p27 in serum-starved cardiomyocytes and REF52 cells exhibited apparently similar kinetics of degradation after serum stimulation (Fig. 3), suggesting no apparent difference of the Skp2-independent degradation between these cells. (iv) Skp2 protein was actively ubiquitylated in cardiomyocytes compared with REF52 cells (Fig. 5*D*). Thus, it is strongly argued that increased Skp2 degradation is one of the mechanisms by which cardiomycytes accumulated p27 in the nuclei and ceased to grow early after the forced cell cycle progression by nuclear cyclin D1.

Other cell cycle inhibitors, p21 and p57, are also recognized and degraded by the Skp2-dependent pathway (25, 26). After cell cycle entry of cardiac cells as well as REF52 cells, p21 was also up-regulated (Fig. 1*B*). However, it was not significantly associated with CDK2 (Fig. 1*C*). Furthermore, p21 degradation in Skp2-expressed cells was less than p27, and p57 was neither induced nor affected significantly by Skp2 expression (Fig. 6*A*). Thus, we speculate it is unlikely that these inhibitors play a major role in cell cycle arrest of D1NLS cardiomyocytes. Inconsistent with this, the knockdown of p27 using the siRNA approach promoted the proliferation of D1NLS/CDK4 cells, indicating that p27 rather than p21 or p57 played a role in causing cell cycle arrest. It is interesting to note here that p27 is highly accumulated with concomitant reduction of cell growth in Skp2-deficient cells (23). In these mice, however, cardiac size or cell number was not significantly affected. In contrast, p27 knockout mice show the enlarged heart with much higher proliferative activity (21). These are consistent with our findings that Skp2 and p27 are reciprocally regulated and the specific p27 down-regulation by siRNA or Skp2 enhanced the proliferation of D1NLS/CDK4 cells. The role of cyclin kinase inhibitors p27, p21, or p57 in suppressing cell cycle progression might depend on the cell type and cellular context. Indeed, it is reported that the expression of these inhibitors in tissue is not uniform (27–29). Thus, more investigation might reveal the functional implication of these inhibitors in cell cycle arrest of terminally differentiated cells.

Cyclin E, which is a component of the late G_1 cyclin kinase CDK2 and is also recognized by Skp2 (23, 30), appeared to be regulated in a biphasic manner. It was up-regulated at low expression of Skp2, but down-regulated at a higher level of Skp2 (Fig. 6*A*). The up-regulation of cyclin E might support cell cycle progression of D1NLS/CDK4/Skp2 cells, whereas its down-regulation at the higher Skp2 level might cause another barrier for cell cycle progression. This is also an another issue of future study.

The heart is developed at the early stage of embryogenesis during which cardiomyocytes retain the ability to proliferate, but they lose the capacity to proliferate in terminal differentiation. Our present study raises an interesting possibility that the down-regulation of Skp2 by increased degradation might be

causally related to the loss of proliferation of cardiomyocytes during terminal differentiation. Inconsistent with this, we observed that fetal rat cardiomyocytes, which decrease cell growth capacity but are still capable of proliferating, exhibited the intermediate activity of the *in vitro* Skp2 ubiquitylation and p27 expression between neonatal cardiac cells and REF52 fibroblasts.[2] More recently, it has been reported that Skp2 and its cofactor Cks1 proteins are degraded by the ubiquitin ligase APC/Ccdh1 (anaphase-promoting complex/cyclosome and its activator Cdh) (31, 32). Detailed analysis of APC expression and its Skp2 degrading activity in cardiomyocytes may clarify the mechanism of terminal differentiation and such an investigation is now in progress.

Finally, we demonstrated that p27 is a strong cell cycle barrier of terminally differentiated cardiomyocytes, and its down-regulation by a combination of p27 siRNA or Skp2 and D1NLS/CDK4 significantly overrode the limited cell proliferation of cardiac cells. The impaired Skp2/p27 regulation may represent one of the molecular mechanisms by which not only cardiomyocytes but also other terminally differentiated cells lose the capacity to proliferate.

REFERENCES

1. MacLellan, W. R., and Schneider, M. D. (2000) *Annu. Rev. Physiol.* **62**, 289–319
2. Chien, K. R., and Olson, E. N. (2002) *Cell* **110**, 153–162
3. Pasumarthi, K. B., and Field, L. J. (2002) *Circ. Res.* **90**, 1044–1054
4. Olson, E. N., and Schneider, M. D. (2003) *Genes Dev.* **17**, 1937–1956
5. Orlic, D., Hill, J. M., and Arai, A. E. (2002) *Circ. Res.* **91**, 1092–1102
6. Beltrami, A. P., Barlucchi, L., Torella, D., Baker, M., Limana, F., Chimenti, S., Kasahara, H., Rota, M., Musso, E., Urbanek, K., Leri, A., Kajstura, J., Nadal-Ginard, B., and Anversa, P. (2003) *Cell* **114**, 763–776
7. Kirshenbaum, L. A., Abdellatif, M., Chakraborty, S., and Schneider, M. D. (1996) *Dev. Biol.* **179**, 402–411
8. Agah, R., Kirshenbaum, L. A., Abdellatif, M., Truong, L. D., Chakraborty, S., Michael, L. H., and Schneider, M. D. (1997) *J. Clin. Investig.* **100**, 2722–2728
9. von Harsdorf, R., Hauck, L., Mehrhof, F., Wegenka, U., Cardoso, M. C., and Dietz, R. (1999) *Circ. Res.* **85**, 128–136
10. Tamamori-Adachi, M., Ito, H., Sumrejkanchanakij, P., Adachi, S., Hiroe, M., Shimizu, M., Kawauchi, J., Sunamori, M., Marumo, F., Kitajima, S., and Ikeda, M. A. (2003) *Circ. Res.* **92**, e12–e19
11. Sherr, C. J., and Roberts, J. M. (1999) *Genes Dev.* **13**, 1501–1512
12. Pagano, M., Tam, S. W., Theodoras, A. M., Beer-Romero, P., Del Sal, G., Chau, V., Yew, P. R., Draetta, G. F., and Rolfe, M. (1995) *Science* **269**, 682–685
13. Sutterluty, H., Chatelain, E., Marti, A., Wirbelauer, C., Senften, M., Muller, U., and Krek, W. (1999) *Nat. Cell Biol.* **1**, 207–214
14. Carrano, A. C., Eytan, E., Hershko, A., and Pagano, M. (1999) *Nat. Cell Biol.* **1**, 193–199
15. Montagnoli, A., Fiore, F., Eytan, E., Carrano, A. C., Draetta, G. F., Hershko, A., and Pagano, M. (1999) *Genes Dev.* **13**, 1181–1189
16. Tsvetkov, L. M., Yeh, K. H., Lee, S. J., Sun, H., and Zhang, H. (1999) *Curr. Biol.* **9**, 661–664
17. Hara, T., Kamura, T., Nakayama, K., Oshikawa, K., Hatakeyama, S., and Nakayama, K. I. (2001) *J. Biol. Chem.* **276**, 48937–48943
18. Nakayama, K. I., Hatakeyama, S., and Nakayama, K. (2001) *Biochem. Biophys. Res. Commun.* **282**, 853–860
19. Ishida, N., Hara, T., Kamura, T., Yoshida, M., Nakayama, K., and Nakayama, K. I. (2002) *J. Biol. Chem.* **277**, 14355–14358
20. Flink, I. L., Oana, S., Maitra, N., Bahl, J. J., and Morkin, E. (1998) *J. Mol. Cell. Cardiol.* **30**, 563–578
21. Poolman, R. A., Li, J. M., Durand, B., and Brooks, G. (1999) *Circ. Res.* **85**, 117–127
22. Tamamori-Adachi, M., Ito, H., Nobori, K., Hayashida, K., Kawauchi, J., Adachi, S., Ikeda, M. A., and Kitajima, S. (2002) *Biochem. Biophys. Res. Commun.* **296**, 274–280
23. Nakayama, K., Nagahama, H., Minamishima, Y. A., Matsumoto, M., Nakamichi, I., Kitagawa, K., Shirane, M., Tsunematsu, R., Tsukiyama, T., Ishida, N., Kitagawa, M., Nakayama, K. I., and Hatakeyama, S. (2000) *EMBO J.* **19**, 2069–2081
24. Yokota, T., Sakamoto, N., Enomoto, M., Tanabe, Y., Miyagishi, M., Maekawa, S., Kurosaki, M., Taira, K., Watanabe, M., and Mizusawa, H. (2003) *EMBO Rep.* **4**, 602–608
25. Bornstein, G., Bloom, J., Sitry-Shevah, D., Nakayama, K., Pagano, M., and Hershko, A. (2003) *J. Biol. Chem.* **278**, 25752–25757
26. Kamura, T., Hara, T., Kotoshiba, S., Yada, M., Ishida, N., Imaki, H., Hatakeyama, S., Nakayama, K., and Nakayama, K. I. (2003) *Proc. Natl. Acad. Sci. U. S. A.* **100**, 10231–10236
27. Zhang, P., Wong, C., DePinho, R. A., Harper, J. W., and Elledge, S. J. (1998) *Genes Dev.* **12**, 3162–3167
28. Dyer, M. A., and Cepko, C. L. (2001) *J. Neurosci.* **21**, 4259–4271
29. Nagahama, H., Hatakeyama, S., Nakayama, K., Nagata, M., Tomita, K., and Nakayama, K. I. (2001) *Anat. Embryol.* **203**, 77–87
30. Yeh, K. H., Kondo, T., Zheng, J., Tsvetkov, L. M., Blair, J., and Zhang, H. (2001) *Biochem. Biophys. Res. Commun.* **281**, 884–890
31. Bashir, T., Dorrello, N. V., Amador, V., Guardavaccaro, D., and Pagano, M. (2004) *Nature* **428**, 190–193
32. Wei, W., Ayad, N. G., Wan, Y., Zhng, G-J., Kirschner, M. W., and Kaelin, W. G., Jr. (2004) *Nature* **428**, 194–198

[2] K. Nobori, M. T-Adachi, and S. Kitajima, manuscript in preparation.

Artificial Organs
29(2):95–103, Blackwell Publishing, Inc.

A New Method for Manufacturing Cardiac Cell Sheets Using Fibrin-Coated Dishes and Its Electrophysiological Studies by Optical Mapping

*Yuji Itabashi, *Shunichiro Miyoshi, *Haruko Kawaguchi, *Shinsuke Yuasa, *Kojiro Tanimoto, *Akira Furuta, †Tatsuya Shimizu, †Teruo Okano, *Keiichi Fukuda, and *Satoshi Ogawa

**Cardiopulmonary Division, Department of Internal Medicine, Keio University School of Medicine, Shinanomachi; and †Institute of Advanced Biomedical Engineering and Science, Tokyo Women's Medical University, Kawada-cho, Shinjuku-ku, Tokyo, Japan*

Abstract: We developed a novel simple method for making functional myocardial cell sheets that may be used as transplants. Polymerized human fibrin-coated dishes were prepared with fibrinogen monomers mixed with thrombin. Neonatal rat cardiomyocytes cultured on these dishes formed myocardial cell sheets within 4 days. These cell sheets were easily dissociated intact from the polymerized fibrin layer, because the fibrin had been digested by intrinsic protease. Two overlaid myocardial cell sheets exhibited synchronized spontaneous beating and captured artificial pacing. Optical mapping confirmed that the conduction of the action potential between two partially overlaid myocardial cell sheets was established, and the action potential propagated across the junction without any delay. Transplanted three-layered myocardial cell sheets exhibited strong spontaneous beating and showed well-differentiated striations and an increase in cell size. This simple method of cell sheet engineering may also be applicable for various other cell types. **Key Words:** Tissue engineering—Cell sheet—Polymerized fibrin—Cardiomyocyte—Optical mapping—Electrical connection.

The use of organ transplantation, a powerful treatment for patients with severely damaged organs, remains limited by the shortage of donors. Recent advances in the field of regenerative medicine now promise possible alternative sources of organ grafts. The regeneration of cardiomyocytes from various stem cells, such as embryonic stem cells (1,2) and bone marrow-derived stem cells (3,4), has been observed in vitro, and a number of cell transplantation therapies have restored the function of damaged cardiac tissues. A clinical trial involving the myocardial injection of autologous myoblasts has produced a limited but important recovery of impaired cardiac function (5,6). However, the direct delivery of isolated cells that were used in these studies can induce some aggregation and necrosis of the grafted cells, and it remains difficult to transplant a sufficient number of cells to significantly improve cardiac function (7,8).

The challenge in tissue engineering has been the production of functional heart grafts with a three-dimensional structure. To maintain the three-dimensional structure of tissues, different scaffolds composed of extracellular matrix and artificial polymers have been tested (9–13). Okano et al. described a unique cell-manipulation technique that could be used to construct three-dimensional myocardial tissues by layering two-dimensional cell sheets. To obtain myocardial cell sheets, they created temperature-sensitive culture dishes by grafting temperature-responsive polymer (poly-N-isopropylacrylamide; PIPAAm) onto the surface of the dish. At 37°C, the surface is hydrophobic, and cells can attach to the dishes. However, when the temperature is dropped to 32°C or below, the surface becomes hydrophilic and the grafted polymer rapidly hydrates. The

Received May 2004; revised July 2004.
Address correspondence and reprint requests to Dr. Keiichi Fukuda, Cardiopulmonary Division, Department of Internal Medicine, Keio University School of Medicine, 35 Shinanomachi, Shinjuku-ku, Tokyo 160-8582, Japan. E-mail: kfukuda@sc.itc.keio.ac.jp

grafted polymer changes to expand, which causes cells to detach from the surface (14,15). This enables the generation of a free, confluent, thin cell sheet just by cooling the dishes to room temperature. Moreover, in contrast to enzymatic digestion, both adhesive proteins and cell–cell junctions between the confluent cells are perfectly preserved with this method, enabling generation of a three-dimensional functional tissue that lacks any scaffold.

We have developed a very simple new cell sheet engineering method using thin biodegradable polymerized fibrin-coated dishes. Here, we describe this new tissue engineering technique, and the histological and electrophysiological characteristics of the myocardial cell sheets. Electrical disconnection between the myocardial cell sheets or between a myocardial cell sheet and a host cardiac tissue may cause fatal arrhythmias (16), so we evaluated the electrical synchronization of engineered myocardial tissue with a high-resolution optical mapping system using a voltage-sensitive dye.

MATERIALS AND METHODS

Preparation of myocardial cell sheets

All experimental procedures and protocols were approved by the Animal Care and Use Committee of Keio University and conformed to the National Institutes of Health Guide for the Care and Use of Laboratory Animals. Tissiel was purchased from Baxter (Vienna, Austria), and its constitution was changed to 90 mg of human fibrinogen, 20 mg of human serum, 0.4 U of thrombin, 0.59 mg of $CaCl_2$ ($2H_2O$), and 3000 U of aprotinin. The solution was diluted with 16 mL of saline, and 0.3 mL was spread rapidly onto 35-mm culture dishes (Becton Dickinson and Company, Bedford, MA, U.S.A.). Two hours later, the polymerized fibrin-coated dishes were obtained, and they were stored at 4°C. Primary cultures of cardiomyocytes were prepared from the ventricles of 1 day-old neonatal Wistar rats (Japan CLEA, Tokyo, Japan) as described previously (17) and were plated on the dishes ($2.8 \times 10^5/cm^2$).

Transplantation of myocardial cell sheets onto adult rat subcutaneous space

The dorsal skin of male F344 nude rats (Japan CLEA) (8 weeks of age, $n = 10$), which were anesthetized by inhalation of diethyl ether (Wako, Osaka, Japan) and subcutaneous injection of 1% procaine-HCL (5–10 mL) (AstraZeneca, London, U.K.), was cut and opened. Then, trilayered myocardial cell sheets were transplanted into the subcutaneous tissue.

Histological analysis

Immunostaining was performed as described previously (18) by using antifibrin (Monosan, Uden, the Netherlands), anti-α-actinin (Sigma, St. Louis, MO, U.S.A.) monoclonal antibodies, and anticonnexin43 (Sigma) polyclonal antibodies. The samples were incubated with either Alexa488-labeled antimouse IgG antibody (Molecular Probes, Eugene, OR, U.S.A.), TRITC-labeled antirabbit IgG antibody (Dako, Tokyo, Japan) or Alexa594-conjugated phalloidin (Molecular Probes Europe BV, Leiden, the Netherlands). Nuclei were stained with TOTO-3 (Sigma). They were observed under confocal laser microscope (LSM510, Carl Zeiss International, Jena, Germany).

Electro-optical analysis of the myocardial cell sheets

For analysis of electrical communication, two myocardial cell sheets were overlapped by 2 mm at the edges and cocultured for 1, 2, and 3 days on culture dishes pretreated with laminin (Roche, Mannheim, Germany) as described previously (19). Extracellular electrical potentials at both ends of each sheet were recorded with a pair of contact bipolar electrodes. The optical mapping system was applied by using a membrane voltage indicator, di-4-ANEPPS (Molecular Probes), to monitor two-dimentional action potential propagation and the electrical connection between the two cocultured myocardial cell sheets. Di-4-ANEPPS stock solution (20 mM) was freshly prepared with DMSO (Sigma) solution containing 20% pluronic F-127 (P-3000, Molecular Probes) and added to the culture media to give a final concentration of 10 μM di-4-ANEPPS. The samples were exposed to the dye at 37°C for 30 min. The plates were then washed in Tyrode's solution consisting of (in mM) 140 NaCl, 4 Cl, 0.5 $MgCl_2$, 1.8 $CaCl_2$, 5 HEPES, 55 D-glucose (pH adjusted to 7.4 with NaOH), and 100 mg/L bovine serum albumin (Sigma). Glucose was then added to adjust the osmotic pressure of Tyrode's solution to the culture media. The myocardial cell sheets were kept in an originally made temperature-controlled chamber (37°C) on the fluorescence microscope (BX50WI, Olympus, Tokyo, Japan). Signals were monitored through a high-resolution CCD-camera system (MiCAM01, 192 × 128 points, 3.5 ms time resolution, Brain Vision, Tokyo, Japan) at an emission wavelength of greater than 610 nm and an excitation wavelength of 520 nm. The sheets were immobilized by cytochalasin-D (25 μM) (Sigma). Action potentials were observed in the case of spontaneous excitation or bipolar pacing via the contact Ag–AgCl electrode. The obtained data were processed accord-

ing to the original procedure (20) using commercial Igor Pro software (Wavemetrics, Inc., Lake Oswego, OR, U.S.A.).

RESULTS

Generation of myocardial cell sheets

The primary cell cultures contained approximately 78% desmin- and connexin43-double-positive cardiomyocytes. After the cells were plated on fibrin polymer-coated dishes (Fig. 1A,B,G), the fibrin layer was gradually degraded by proteases secreted from the cultured cells (Fig. 1C). After 4 days, the myocardial cell sheets were detached from the plates with a cell scraper (Fig. 1D,H), laid flat in culture media (medium 199/DMEM supplemented with 10% FBS) (Fig. 1E,I), then trimmed to a square shape and overlaid for subsequent experiments (Fig. 1F,J).

Histological analysis of myocardial cell sheets obtained from the polymerized fibrin-coated dishes

To assess the myocardial cell sheets obtained by this method, we collected the cells with a scraper at various time points after plating of the cardiomyocytes on the polymerized fibrin-coated dishes (Fig. 2). When the myocardial cell sheets were peeled off from the dishes after 4 days, the detached myocardial cell sheets decreased in diameter by $38 \pm 3.6\%$ ($n = 30$). Myocardial cell sheets could not be obtained by using noncoated, gelatin-, laminin-, or fibronectin-coated culture dishes (data not shown). We defined the time from the primary culture to the fabrication of the myocardial cell sheets as PX days, and the time from the fabrication to the experiment as SX days (Fig. 2A). Residual fibrin polymer was observed at the bottom of the sheet in the sample obtained on day 4 (P4–S0) (Fig. 2B), but was not detected in the sample taken on day 6 (P6–S0) (Fig. 2C). Fibrin polymer was still visible in the interstitial space in the P4–S1 sheet (Fig. 2D,F) but was completely digested in the P4–S3 sheet (Fig. 2E,G). When aprotinin (serine protease inhibitor) was added (600 KIU/mL) to the samples after separation of the cell sheets, a considerable amount of fibrin polymer was observed to have remained undigested (Fig. 2H–K).

Characteristics of the myocardial cell sheet made using the fibrin-coated dish

To investigate the optimal time to harvest the myocardial cell sheets after primary culture, we collected the cells with a scraper at various time points after plating the cardiomyocytes on the polymerized fibrin-coated dishes ($n = 12$ each, Fig. 3A). The

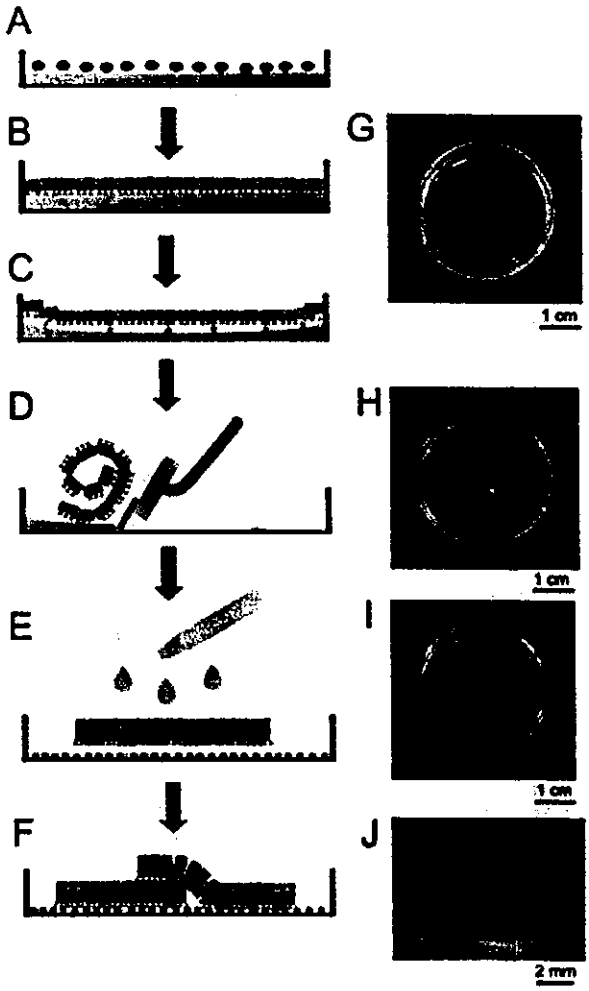

FIG. 1. Representative schema of the manipulation of myocardial cell sheets using polymerized fibrin-coated dishes. (A) Primary cultured neonate rat cardiomyocytes were spread onto the polymerized fibrin-coated dishes. (B,G) Cardiomyocytes became confluent. (C) In 4 days, the fibrin polymer had been degraded by proteases secreted from cardiomyocytes. (D) Cells were gently raked from the edge toward the center of the dishes so as not to tear the myocardial cell sheets with the cell scraper. (H) Shrunken myocardial cell sheets were obtained. (E,I) A few drops of culture media were applied to the shrunken sheets to unfold them. (F,J) The edges of the flattened myocardial cell sheets were trimmed into a square shape by using a blade. In some experiments, two myocardial cell sheets were overlaid at the margin with 2-mm width and co-cultured on laminin-coated culture dishes.

success rate for obtaining myocardial cell sheets increased after 3 days and peaked at day 4 (100% success rate).

The percentage of spontaneous beating of the myocardial cell sheets was then taken at different time intervals ($n = 12$ each). We first altered the duration of PX days while keeping SX days fixed to 3 (S3 day). The percentage of beating myocardial cell

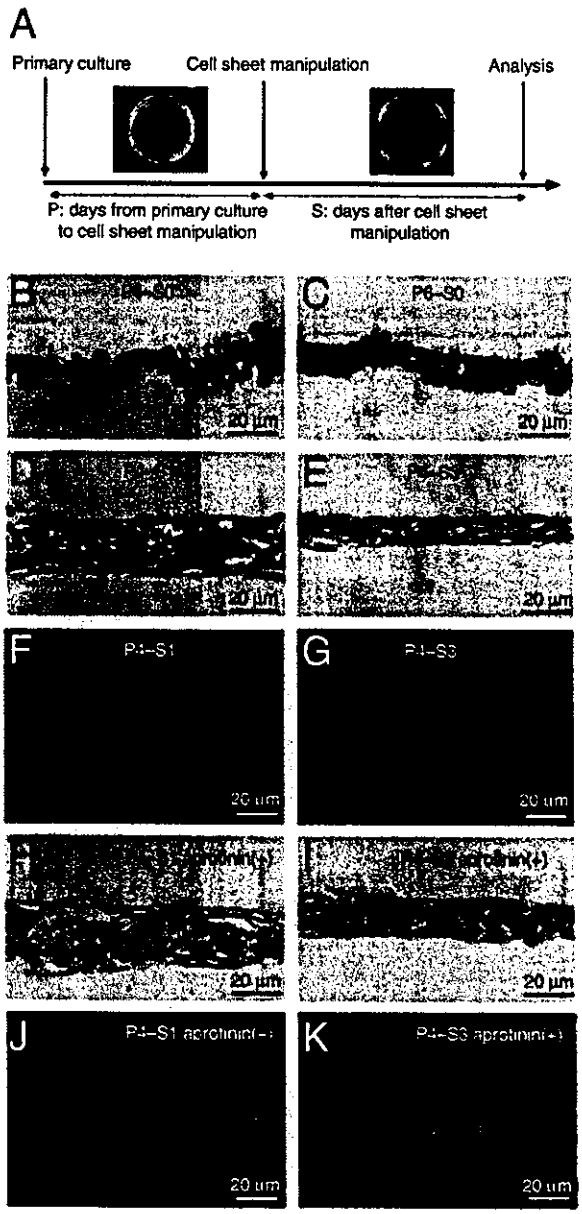

FIG. 2. Histological analysis of the myocardial cell sheets. (A) Protocol for making the myocardial cell sheets and definition of PX and SX days. (B–E,H,I) Hematoxylin and eosin staining of the myocardial cell sheets. (F,G,J,K) Immunofluorescent staining of the myocardial cell sheets. Red: F-actin; Green: fibrin; Blue: TOTO-3 indicating nuclei. Protocols and scale bars are indicated in the figure inset.

sheets showed that the difference in PX days did not affect the percentage (Fig. 3B).

Next, we fixed the PX to 4 days (P4 day), changed the length of SX days, and again measured the percentage of spontaneous beating of the cell sheets ($n = 30$). The percentage of spontaneous beating began to increase significantly from S2 day and reached 100% at S6 day (Fig. 3C). Furthermore, the percentage of myocardial cell sheets that captured artificial pacing increased from S2 day and reached 100% at S5 day (Fig. 3D).

Figure 3(E) shows the beating rate of the myocardial cell sheets from S0 day. It increased rapidly to S3 day and continued to increase at a slower rate thereafter ($n = 6$).

Inasmuch as we could reach 100% of the success rate on P4 day and P5 day, and responsiveness to artificial pacing increased remarkably for the first 3 days, the P4–S3 sheet appeared to have established relatively stable electrical nature.

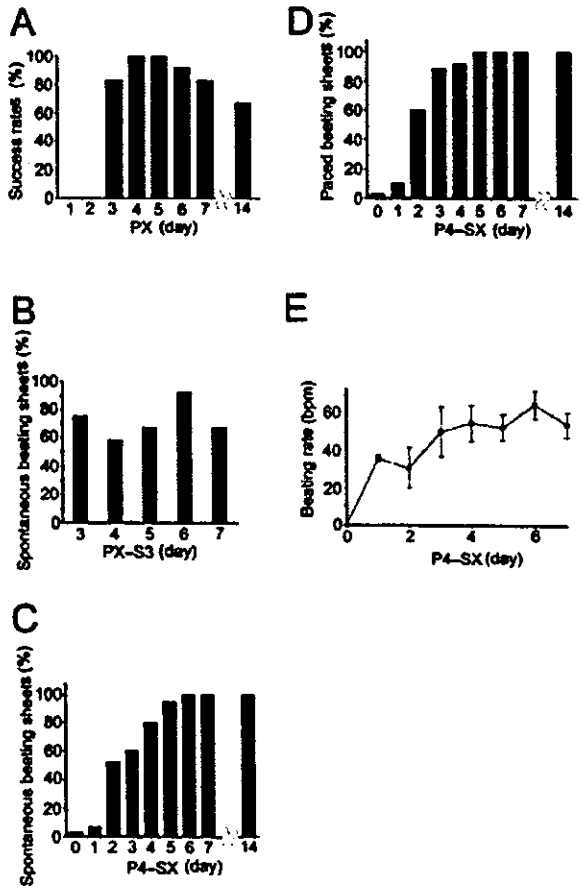

FIG. 3. Characterization of the myocardial cell sheets. Abbreviations in the figures (PX, PX–S3, P4–SX) were explained at Fig. 2(A). (A) Rate of success of obtaining myocardial cell sheets in the PX day sample. (B) Percentage of spontaneously beating myocardial cell sheets in the PX–S3 day samples. (C) Percentage of spontaneously beating sheets in the P4–SX day samples. (D) Percentage of myocardial cell sheets that captured artificial pacing in the P4–SX day samples. (E) The rate of beating in the P4–SX day samples. Values are presented as mean ± SEM.